Load Tests and Numerical Modeling of CFA and Driven Piles in Marl in Savannah, Georgia

by

Zhihao Zhou
B.Eng., Sichuan University, China, 2018
M.Sc., Nanyang Technological University, Singapore, 2019

A Thesis Submitted in Partial Fulfillment of the
Requirements for the Degree of

MASTER OF APPLIED SCIENCE

in the Department of Civil Engineering

Supervisory Committee

Load Tests and Numerical Modeling of CFA and Driven Piles in Marl in Savannah, Georgia

by

Zhihao Zhou
B.Eng., Sichuan University, China, 2018
M.Sc., Nanyang Technological University, Singapore, 2019

Supervisory Committee

Dr. Cheng Lin, Supervisor
Department of Civil Engineering

Dr. Min Sun, Departmental Member
Department of Civil Engineering

Abstract

Marl along the southeast coast of the US, especially in South Carolina and Georgia, is a stiff, calcium carbonate-rich, over-consolidated fine-grained soil commonly used as a bearing layer for pile foundations. However, two significant engineering challenges arise: unreliable CPT-based estimations of pile resistance and strain-softening behavior complicating the prediction of pile capacity, deformation, and load-transfer mechanisms under axial load.

Comprehensive pile load tests conducted in Savannah, Georgia, were used to improve CPT-based pile resistance estimations and develop a numerical model using load-transfer (*t-z* and *Q-z*) method for driven and Continuous Flight Auger (CFA) piles. For CPT-based pile resistance estimations, the accuracy of the original LCPC and Eslami and Fellenius methods was first evaluated. Pile load test results were then used to back-calculate the coefficients of these methods for improvement, which were subsequently verified with additional pile load test data. The main strength parameters of the load-transfer (*t-z* and *Q-z*) method model were correlated with the improved CPT methods coefficients. After calibration, the numerical model was verified using additional pile load test data. Moreover, a 3D continuum finite element method (FEM) simulation using the 'OC Clay' model in Plaxis 3D was conducted to capture strain-softening behavior and examine load-transfer mechanisms. The 3D continuum FEM model was calibrated and validated against separate pile load test data, and a parametric study was conducted to investigate how soil strength parameter, pile dimensions, and embedment depth into marl influence pile performance.

Keywords

Marl; Driven pile; CFA pile; Numerical simulation; *t-z* method; CPT correlation; 3D continuum finite element method

Table of Contents

List of Tables

List of Figures

Notations

A_p = cross-sectional area of pile

a_p = pore pressure adjustment factor

a, b, and c = empirical coefficients in *t-z* curve

a_t, b_t, and c_t = empirical coefficients in *Q-z* curve

B = diameter/side length of the pile

β_t = the ratio of the residual toe resistance to the ultimate toe resistance *Q-z* curve

β_s = the ratio of the residual unit shaft resistance to the ultimate unit shaft resistance in *t-z* curve

C_s = empirical correlation coefficient for shaft resistance (dimensionless) of Eslami and Fellenius method

C_t = empirical correlation coefficient for toe resistance (dimensionless) of Eslami and Fellenius method

E_{oed} = oedometer modulus

E_p = pile modulus

E_{ur} = unloading-reloading Young's modulus

E' = Young's modulus

el_{Reload} = flag to switch from an elasto-plastic response during reloading paths (el_{Reload} =0), to an elastic behavior in OC Clay model

f_s = ultimate shaft resistance

f_{sm} = the upper limit of f_s

φ'_{cs} = critical state friction angle

φ' = effective friction angle

G_0 = small strain shear modulus

G_s = secant shear modulus

γ = unit weight of soil

$\gamma^{0.7}$ = threshold shear strain at which the secant shear modulus $G_s = 0.722G_0$

h = parameter introduced to increase/decrease the plastic deformability of the soil

k_1 and k_2 = two slopes of the bilinear curve

K_0 = earth pressure coefficient at rest

K_s = empirical correlation coefficient for shaft resistance (dimensionless) of LCPC method

K_t = empirical correlation coefficient for toe resistance (dimensionless) of LCPC method

L_p = pile length

L_b = pile embedment length

L_e = embedment length into marl

OCR = over-consolidation ratio

P_h =load applied at the pile head

p^{ref} = reference mean effective stress

POP = pre-overburden pressure

q_b = pile-soil interface toe resistance

q_c = uncorrected CPT tip resistance

q_{ca} = the average value of CPT q_c from below to above 1.5B relative to the pile toe, where B is pile side width or diameter

q_E = cone resistance after correction for pore pressure on the cone shoulder and adjustment to apparent “effective” stress

q_{Eg} = the geometric average of the q_E over the influence zone

q_T = cone resistance adjusted for pore water pressure on shoulder

q_t = toe resistance

Q = toe resistance provided by soil in Q-z curve

Q_u = the ultimate pile toe resistance in Q-z curve

Q_1 = the load corresponding to the 6.4 mm settlement level

Q_2 = the load corresponding to the point obtained by the tangential method

Q_3 = the load corresponding to the point where the line makes an angle of 0.025 mm/kN intersects with the load-settlement curve

R_{ca} = a ratio of pile circumference to cross-sectional area

σ_v', max = maximum value due to pre overburden pressure

σ_v = vertical stress in the soil

σ_v' = vertical effective stress in the soil

τ_s = shaft resistance at a given depth, z in t-z curve

u = pile head vertical displacement

U_2 = pore pressure measured at cone shoulder

u_t = displacement at the pile toe in Q-z curve

u_{su} = the displacement at the ultimate shaft resistance in Q-z curve

v_{ur} = Poisson's ratio in unloading and reloading

v = Poisson's ratio

z = depth below pile head

Acknowledgments

I am immensely grateful to my supervisor, Dr. Cheng Lin, for his exceptional guidance, support, and encouragement throughout my research journey. His provision of research facilities and his willingness to share his vast knowledge and consulting experience were invaluable. Dr. Lin's patient mentorship was crucial in helping me navigate the entire research process. This thesis would not have been possible without his insightful guidance. I also deeply appreciate his encouragement, which has greatly influenced both my academic progress and personal development.

Dedication

To my parents, for your unwavering love and support throughout this journey.

To my colleagues in Lin's Lab, for your encouragement and companionship during the toughest times.

And to all the staff in the Department of Civil Engineering, for your support in fostering a conducive environment for my studies.

Chapter 1

1. Introduction

1.1 Background

Marl is a deposit characterized by carbonate-rich, calcareous, overconsolidated soil high in calcium. Marl along the southeast coast of the U.S., particularly in South Carolina and Georgia, is characterized by stiff, calcium carbonate-rich, over-consolidated fine-grained soil. Due to its long-term deposition over millions of years, this marl exhibits consistent soil properties, making it a preferred bearing layer for pile foundations, in contrast to the younger, denser sands and alluvial soft clays above it. However, designing piles in this stiff marl presents two significant challenges. Firstly, CPT-based estimations for pile shaft and toe resistance are often unreliable, necessitating reliance on pile load test results or empirical values from other sites, which may not be reliably extrapolated. Secondly, the strain-softening behavior of over-consolidated marl complicates numerical simulations, making accurate predictions of pile capacity and deformation under axial loads challenging.

The mostly used approach for capacity analysis, Cone Penetration Test (CPT) methods such as the LCPC (Bustamante and Gianeselli, 1982) and Eslami and Fellenius methods (Eslami and Fellenius, 1997) are often too conservative and unreliable when applied to this material (Tan and Lin, 2014). Earlier studies, such as those by Baus and Ray (1988), have attempted to develop direct CPT correlations for estimating pile resistance in stiff marl. However, these correlations have not been effective for the stiff marl found in Savannah. As such, local engineers tend to rely on the shaft resistance and toe resistance derived from pile load tests, including static and dynamic load

tests. However, performing pile load tests is cost-prohibitive for most projects. In these circumstances, empirical estimations using data from past load test projects are commonly applied for pile design, as demonstrated by Camp and Parmar (1999) and Lin and Lin (2019). Thus, the first aim of this paper is to assess the applicability of current CPT based methods and improve the design of piles in stiff marl by proposing better CPT-based pile resistance estimations.

The design of piled foundations in marl often overlooks load-transfer mechanisms and deformation behaviors, focusing mainly on capacity. However, relying solely on 'capacity' is inadequate due to its variable definitions and the impact of static load test methods (Fellenius, 2013; 2017). Simply applying safety factors to capacity does not accurately predict a pile's response to working loads. Instead, analyzing static load test results in terms of load-movement response is essential. This approach allows for theoretical simulations that better predict how the pile will behave under applied loads (Fellenius and Rahman, 2019).

To study load-transfer mechanisms and deformation behaviors, researchers have introduced various methods to analyze the response of compression piles. These methods include full-scale pile load tests, dynamic energy or pile-driving formulas, numerical methods, analytical approaches based on in-situ testing (e.g., cone penetration test (CPT), standard penetration tests (SPT), and dilatometer tests (DMT)), shear strength properties from direct shear or triaxial laboratory tests, and artificial neural networks (Shalabi et al. 2023). Each approach has its own advantages and disadvantages. For instance, full-scale pile load tests (Fellenius et al., 2004; Fellenius, 2021; Fellenius and Ruban, 2020; Amini et al., 2008**)** are widely used but are costly, as discussed above. Dynamic energy or pile-driving formulas (Rausche et al. 1985, Benamar 2000) are often limited by cost, time, and equipment constraints. Artificial neural networks are a newer method and can

produce diverse and sometimes confusing results (Shalabi et al. 2023). Among these, numerical modeling is considered an efficient and cost-effective approach.

Numerical simulation methods, such as the load-transfer curve method (*t-z* and *Q-z* methods), utilize the finite difference approach to discretize a pile into segments influenced by shaft shear or toe stress (Fellenius and Rahman 2019). Widely applied in both industry and research, these methods predict the load-settlement response and load-transfer mechanisms of piles under axial load without extensive pile load tests. Factors influencing *t-z* behavior include pile diameter, axial stiffness, pile length, and soil strength and stiffness (Kraft et al., 1981). The load-transfer function, controlled by a function coefficient, expresses load as a function of movement through a nonlinear relationship (Fellenius and Rahman 2019). The *t-z* and *Q-z* curves are represented by soil springs at the pile shaft and toe, respectively, and are specific to soil type. For instance, shaft reactions in sands (*t-z* curves) follow a hyperbolic relationship (Lee and Xiao, 2001; Zhang et al., 2014; Xiao et al., 2002; Yetginer et al., 2006), while in soft clays, they follow a power law (Williamson, 2014; Vardanega, 2015; Crispin et al., 2019) or exponential function (Wang et al., 2012). Toe response (*Q-z* curves) in sands is modeled using a hyperbolic relationship (Xiao et al., 2002) or bilinear model (Zhang et al., 2014), while in soft clays, it follows an exponential function (Wang et al., 2012). However, these methods do not directly address the axial responses of piles in marl, which exhibit strong strain softening, leading to pile plunging. Research on this specific issue is scarce. Moreover, although the 3D continuum finite element method (FEM), integrated into commercial software like Plaxis 3D, is more straightforward, as it visualizes complex interactions and results directly through an intuitive interface, few studies focus on finite element modeling of axially loaded pile tests in stiff marl. Therefore, it is essential to adopt the 3D continuum FEM to simulate the response of piles embedded in stiff marl under axial load. An 3D continuum FEM an provide

accurate simulations that address the strain-softening characteristics of marl, thereby enhancing the understanding and prediction of pile behavior in such challenging conditions. Additionally, the 3D continuum FEM is ideal for parametric studies, extending the understanding of pile performance sensitivity to soil parameters and pile dimensions, and optimizing pile design by identifying the most influential variables for cost-effective and efficient foundation solutions.

In conclusion, this study aimed to improve pile design in stiff marl by proposing enhanced CPT-based pile resistance estimations for driven piles and CFA piles. Furthermore, the study developed a new load-transfer (*t-z* and *Q-z*) method model to deepen the understanding of the deformation response and load-transfer mechanism of piles embedded in stiff marl. Additionally, this study explores the use of an advanced constitutive model in 3D continuum FEM, followed by a parametric study using the FEM model.

1.2 Objective and scope of this study

The main objectives of this study are to:

(1) establish accurate CPT based correlations for driven piles and CFA piles resistance prediction in stiff marl

(2) propose a load-transfer (*t-z* and *Q-z*) method for better capturing the strain-softening response of driven piles and CFA piles in marl

(3) develop a 3D continuum FEM using an advanced constitutive model to capture the strain-softening feature of driven piles in stiff marl and investigate the impact of marl strength properties and pile dimensions on pile response through parametric study

1.3 Structure of this thesis

This thesis is based on two manuscripts presented in Chapters 2 and 3. Chapter 2 focuses on improving the CPT-based method and proposing a load-transfer method to better capture the strain-softening response of piles in stiff marl. Chapter 3 involves the development of a 3D continuum FEM model along with a parametric study.

The structure of this thesis is as follows:

Chapter 1 presents a general introduction, which addresses the background, objective and scope of this study.

Chapter 2 evaluates the performance of existing CPT based methods, such as the LCPC and Eslami and Fellenius methods, against actual load test results and proposes adjustments to enhance their accuracy. The chapter also introduces a numerical model using the proposed $t{-}z$ and $Q{-}z$ curves to predict pile behavior in marl, which is calibrated with load test data. Additionally, the chapter verifies the numerical model using additional pile tests and analyzes the model's accuracy. Potential sources of error in numerical modeling and CPT data interpretation are discussed, and the implications of the developed model are provided. The chapter concludes with a summary of key findings.

Chapter 3 presents an advanced 3D continuum finite element method analysis using Plaxis 3D to capture strain-softening behavior and understand the axial capacity, settlement behavior, and load transfer mechanisms of driven piles in stiff marl. The 'OC Clay' model is employed to evaluate these interactions. The model is calibrated and validated against pile load test data, followed by a parametric study investigating the effects of critical state friction angle, pile side length, and embedment length.

Chapter 4 summarizes and concludes this research, offering key insights and findings.

References

Amini, A., Fellenius, B. H., Sabbagh, M., Naesgaard, E., and Buehler, M. (2008). "Pile loading tests at Golden Ears Bridge." 61st Canadian Geotechnical Conference, Edmonton, September 21-24, 2008, 8 p.

Baus, R.L., and Ray, R.P. (1988). "Axial pile capacity study for piles in calcareous marl." Engineering for Calcareous Sediments, Jewell & Andrews, eds., Balkema, Rotterdam, Netherlands, 219-226.

Benamar, A. (2000). "Dynamic pile response using two pile-driving techniques." Soil Dynamics and Earthquake Engineering, 20(4), 243-247.

Bustamante, M., and Gianeselli, L. (1982). "Pile bearing capacity prediction by means of static penetrometer CPT." Proc., Second European Symp. on Penetration Testing, May 24-27, 1982, Amsterdam, Laboratoire Central des Ponts et Chaussées, Paris, France.

Camp, W. M., and Parmar, H. S. (1999). "Characterization of pile capacity with time in the Cooper Marl: Study of applicability of a past approach to predict long-term pile capacity." Transp. Res. Rec., 1663(1), 16-24.

Crispin, J. J., Vardanega, P. J., and Mylonakis, G. (2019). "Prediction of pile settlement using simplified models." Proc., XVII ECSMGE-2019: Geotechnical Engineering foundation of the future, Article 0388, Icelandic Geotechnical Society.

Eslami, A., and Fellenius, B. H. (1997). "Pile capacity by direct CPT and CPTu methods applied to 102 case histories." Can. Geotech. J., 34(6), 886-904.

Fellenius, B. H., Harris, D. E., and Anderson, D. G. (2004). "Static loading test on a 45 m long pipe pile in Sandpoint, Idaho." Can. Geotech. J., 41(4), 613-628.

Fellenius, B. H. (2013). "Capacity and load-movement of a CFA pile: A prediction event." ASCE GeoInstitute Geo Congress San Diego, March 3-6, 2013, Foundation Engineering in the Face of Uncertainty, ASCE, Reston, VA, James L. Withiam, Kwok-Kwang Phoon, and Mohamad H. Hussein, eds., Geotechnical Special Publication, GSP 229, pp. 707-719.

Fellenius, B. H. (2017). "Report on the B.E.S.T. prediction survey of the 3rd CBFP event." Proc., 3rd Bolivian Int. Conf. on Deep Foundations, Santa Cruz de la Sierra, Bolivia, April 27-29, Vol. 3, 7–25.

Fellenius, B. H., and Rahman, M. M. (2019). "Load-movement response by *t-z* and *q-z* functions." Geotech. Eng. J. of the SEAGS & AGSSEA, 50(3), 11–19.

Fellenius, B. H., and Ruban, T. (2020). "Analysis of strain-gage records from a static loading test on a CFA pile." Journal of the Deep Foundation Institute, 14(1), 39-44.

Fellenius, B. H. (2021). “Comments on analysis of a static loading tests.” IPA, Invited Special Contribution, 6(3), 23-30.

Kraft, L. M., Ray, R. P., and Kagawa, T. (1981). “Theoretical *t-z* curves.” J. Geotech. Eng. Div., 107(11), 1543–1561.

Lee, K. M., and Xiao, Z. R. (2001). “A simplified nonlinear approach for pile group settlement analysis in multilayered soils.” Can. Geotech. J., 38(5), 1063–1080.

Lin, G. M., and Lin, C. (2019). “Driven pile supported LNG tank in Savannah, Georgia.” Deep Foundation Institute Magazine, Jan/Feb Issue (cover feature) (invited article).

Rausche, F., Goble, G.G., and Likins, G.E. Jr. (1985). “Dynamic determination of pile capacity.” Journal of Geotechnical Engineering, 111(3), 367-383.

Shalabi, F. I., Saleem, M. U., Qureshi, H. J., Arifuzzaman, M., Khan, K., and Rahman, M. M. (2023). “3D FE analysis of bored pile-pile cap interaction in sandy soils under axial compression- parametric study.” Journal of Engineering Research, 11, 301-313.

Tan, Y., and Lin, G. (2014). “Comprehensive load test on prestressed concrete piles in alluvial clays and marl in Savannah, Georgia.” J. Perform. Constr. Facil., 28(1), 178-190.

Vardanega, P. J. (2015). “Sensitivity of simplified pile settlement calculations to parameter variation in stiff clay.” In M. G. Winter, D. M. Smith, P. J. L. Eldred, and D. G. Toll, eds., Geotechnical Engineering for Infrastructure and Development: Proc., XVI European Conf. on Soil Mech. and Geotech. Eng., 7, 3777–3782. Thomas Telford, London.

Wang, Z., Xie, X., and Wang, J. (2012). “A new nonlinear method for vertical settlement prediction of a single pile and pile groups in layered soils.” Comput. Geotech., 45, 118–126.

Williamson, M. G. (2014). “Tunnelling effects on bored piles in clay.” Doctoral thesis, University of Cambridge, Cambridge, U.K.

Xiao, H. B., Luo, Q. Z., Tang, J., and Li, Q. S. (2002). “Prediction of load-settlement relationship for large-diameter piles.” Struct. Design Tall Build., 11(4), 285–293.

Yetginer, A. G., White, D. J., and Bolton, M. D. (2006). “Field measurements of the stiffness of jacked piles and pile groups.” Géotechnique, 56(5), 349–354.

Zhang, Q., Li, L., and Chen, Y. (2014). “Analysis of compression pile response using a softening model, a hyperbolic model of skin friction, and a bilinear model of end resistance.” J. Eng. Mech., 140(1), 102–111.

Chapter 2

2. Load Tests and Numerical Modeling of CFA and Driven Piles in Marl in Savannah, Georgia

2.1 Introduction

Marl along the southeast coast of the US such as South Carolina and Georgia is characterized with a stiff, calcium carbonate rich, over-consolidated fine-grained soil. It is often used as a bearing layer for pile foundations in this region because the marl has been deposited for millions of years, exhibiting relatively consistent soil properties as compared with the younger deposits above it such as dense sands and alluvial soft clays. Two engineering challenges are presented when designing piles in the stiff marl. Firstly, the widely used CPT based estimation of pile shaft resistance and toe resistance in the marl is unreliable, and engineers often resort to the pile load test results or the empirical values derived from past pile load tests in other sites. The extrapolation of the numbers from one site to another site may not reliable. Secondly, the strain softening behavior of the over-consolidated marl poses challenge in numerically simulating piles in practice, complicating the accurate prediction of pile capacity and deformation under axial loads.

Existing CPT-based methods for pile axial capacity, such as the Laboratoire Central des Ponts et Chaussées (LCPC) method (Bustamante and Gianeselli, 1982) and Eslami-Fellenius method (Eslami and Fellenius, 1997), are often too conservative and less reliable when applied to marl in coastal Georgia (Tan and Lin, 2014). As such, local engineers tend to rely on the shaft resistance and toe resistance derived from the pile load tests including static and dynamic load tests. However, performing pile load tests is cost prohibitable for most projects. In such a circumstance, the

empirical estimation using the dataset for past load test projects is commonly applied for the pile design: e.g., Camp and Parmar (1999) and Lin and Lin (2019).

In contrast to the capacity, load-transfer mechanisms and deformation behaviors of piles in marl are less considered in practice. Designing a piled foundation requires balancing safety, serviceability, and economy. Relying solely on 'capacity' is insufficient due to varying definitions of capacity and the influence of static load test methods (Fellenius, 2013; 2017). Moreover, simply downgrading capacity with safety factors does not predict the pile's response to working loads. Instead, static load test results should be analyzed in terms of load-movement response, enabling a theoretical simulation to assess how the pile will react to applied loads (Fellenius and Rahman, 2019).

The common methods for settlement and load-transfer behavior of piles under axial loading include the load-transfer curve method (e.g., Kraft et al., 1981), also known as *t-z* and *Q-z* method and continuum finite element method or finite difference method. Due to the simplicity, the former is more widely adopted in practice. The *t-z* and *Q-z* curves are simply presented by soil springs at pile shaft and pile toe, respectively, which however, are soil specific. For example, the shaft reaction of pile in sands (i.e., *t-z* curves) are simulated by hyperbolic relationship (Lee and Xiao, 2001; Zhang et al., 2014; Xiao et al., 2002; Yetginer et al., 2006) while that in soft clays by power law relationship (Williamson, 2014; Vardanega, 2015; Crispin et al., 2019) or exponential function (Wang et al., 2012). For the toe response (i.e., *Q-z* curves), hyperbolic relationship (Xiao et al., 2002) or bilinear model (Zhang et al., 2014) is applied for pile toe in sands while the exponential function (Wang et al., 2012) is used for pile toe in soft clays. Nevertheless, none of the above directly addresses the axial responses of piles in marl, which, as previously discussed, presents strong strain softening and thus causing the pile plunge. For the continuum finite element method,

simulating the pile plunge is typically difficult due to the strain softening. As such, a scarcity of research has been focused on this issue.

This research aims to improve the design of piles in stiff marl by proposing a better CPT-based pile resistance estimation and a new load-transfer (*t-z* and *Q-z*) method. The proposed approaches apply to both driven concrete piles and displacement continuous flight augered (CFA) piles in marl. The methods were developed based on the results from a comprehensive pile load test program at one site and further verified using the data from another site. This paper first describes the program of pile load tests on driven concrete piles and displacement CFA piles in Savannah, Georgia USA, followed by developing the methods for calculating ultimate resistance and displacement of these piles in marl. The outcomes of this study only not provide a comprehensive dataset for pile responses in stiff marl that will be of great value for calibration or verification of numerical models, but also contribute to the improved design methodology for axially loaded piles in stiff marl.

2.2 Subsurface conditions

The project was located on an island in Savannah, Georgia USA. Its objective was to construct a natural gas liquefaction plant to convert natural gas to liquefied natural gas (LNG). This conversion would reduce the natural gas volume by approximately 600 times and thus facilitate its storage and transportation.

As part of this LNG project, pile foundations were constructed to support the infrastructure required for liquefying natural gas. A comprehensive pile test program was conducted to develop recommendations for pile design and construction. The pile load tests aimed to achieve the following objectives: (1) assessing the constructability of the piles considered for the project, including continuous flight auger piles (CFA), driven precast prestressed concrete (PSC) piles, and

steel H piles; (2) establishing pile capacities in compression, tension, and lateral load for foundation design; (3) determining installation procedures to inform the development of a quality control program for production piles. The pile test program was conducted mainly in two test areas within the project site: test area 1 (T1) and test area 2 (T2), which are approximately 650 m apart. These areas were chosen because their subsurface conditions represented the two extreme soil conditions present within the project's footprint. A test pad was constructed in T1 to raise the ground elevation from the original 3.2 m above the datum of mean low water (MLW) to the design 4.5 m MLW. In contrast, test area 2 had a crust layer at the surface and its ground elevation was close to the design ground elevation. Therefore, no test pad was included in this area.

Prior to the pile load tests, a comprehensive subsurface investigation program was implemented, which included cone penetration tests (CPTs), standard penetration tests (SPTs), dilatometer tests (DMTs), geophysical tests (e.g., multichannel analysis of surface waves, MASW, and seismic CPTs) and a series of laboratory tests such as index property tests, oedometer tests, and triaxial tests. The results of the subsurface investigation program are presented in Fig. 2-1. In general, the subsurface consisted of a very soft to soft alluvial clay layer, over a medium dense to dense sand layer, and a stiff marl. The top of the marl was located at depths of 21 and 15.5 m below the surface in test areas 1 and 2, respectively. The sand layer was missing in Area 2, resulting in a shallower depth of marl surface in test area 2 than in test area 1. As a Miocene geological formation, marl is a relatively uniform and reliable stratum than the above soft clays and/or sands, and thus is generally considered as a pile bearing layer in the Savannah area as well as along the coast of Georgia and South Carolina.

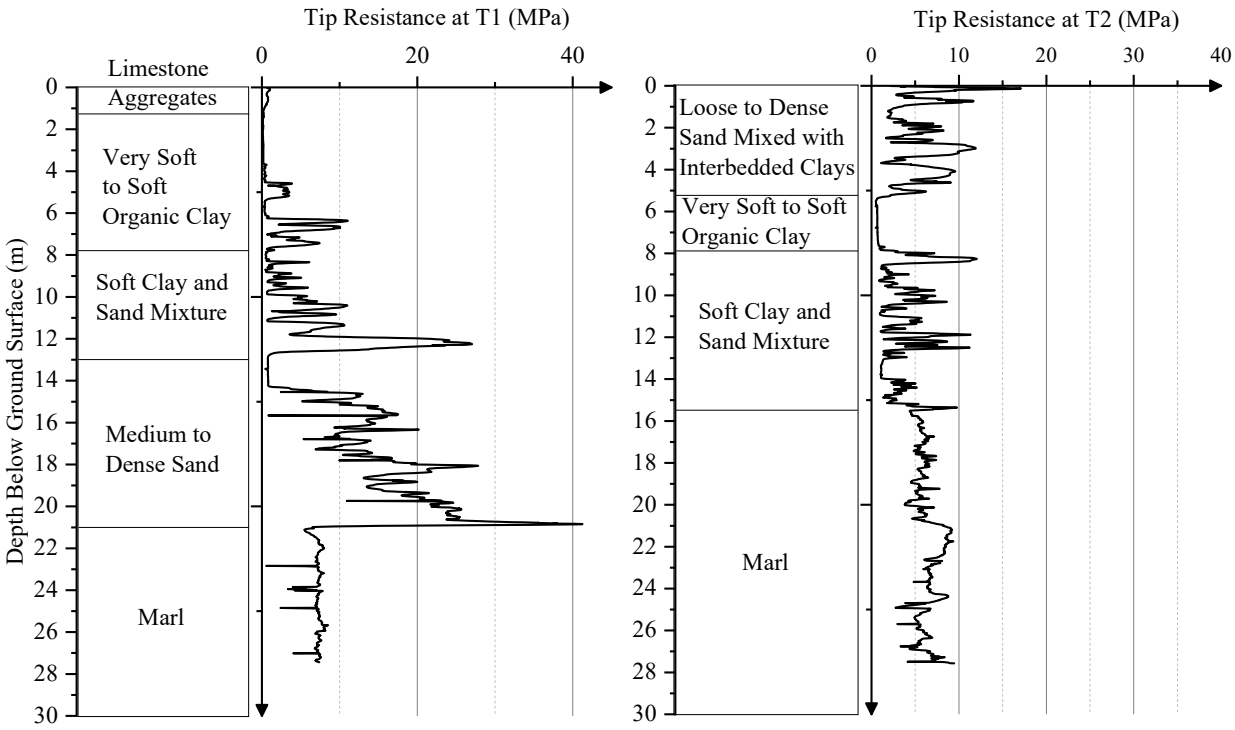

Fig. 2-1. Subsurface conditions along with CPT tip resistance for T1 and T2

2.3 Pile load test program

The test piles for this study were comprised of driven concrete piles and CFA piles. The driven concrete piles were square prestressed concrete (PSC) piles. The CFA piles included full displacement augered cast in place (DACIP) piles and partial displacement augered cast in place (PACIP) piles. A DACIP pile uses a continuous flight auger with a displacement tool to laterally displace soil as it drills down. The auger is reversed at the top to minimize soil spoil, and grout or concrete is pumped through the hollow stem as it is withdrawn. This method minimizes soil spoil and increases the surrounding soil density. In contrast, a PACIP pile uses a continuous flight auger that partially displaces and partially removes soil. The auger excavates soil while some is displaced laterally. Grout is pumped through the hollow stem during withdrawal, balancing soil removal and

displacement, making it suitable for various soil conditions. Fig. 2-2 illustrate the drilling tools and installation mechanisms for PACIP and DACIP, respectively. Test area 1 contained a 0.46 m (i.e., 18-inch) square PSC test pile denoted as T1-18PSC, a DACIP test pile denoted as T1-D1, and a PACIP test pile denoted as T1-P1. The embedment length of the test piles was approximately 24.4 m (i.e., 80 feet) below the ground surface (i.e., the test pad surface), with the pile toe being approximately 3.4 m into the marl. Test area 2 contained a 0.36 m (i.e., 14-inch) square PSC pile (T2-14PSC), a 0.46 m (i.e., 18-inch) DACIP pile (T2-D1), and a PACIP test pile (T2-P1). The embedment length of the test piles was approximately 19.8 m (i.e., 65 feet), with the pile toe being 4.3 m into the marl. The layouts of the test areas and test piles are shown in Figs. 2-3 and 2-4 (a) and (b). Detailed test pile information is presented in Table 2-1.

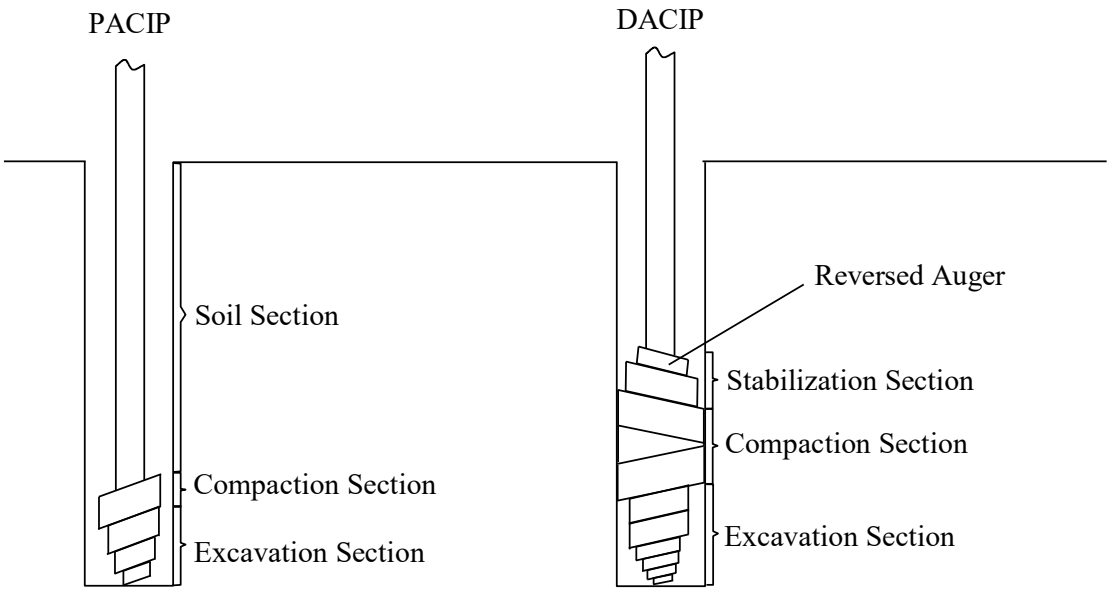

Fig. 2-2. Drilling tools and installation mechanisms for PACIP and DACIP

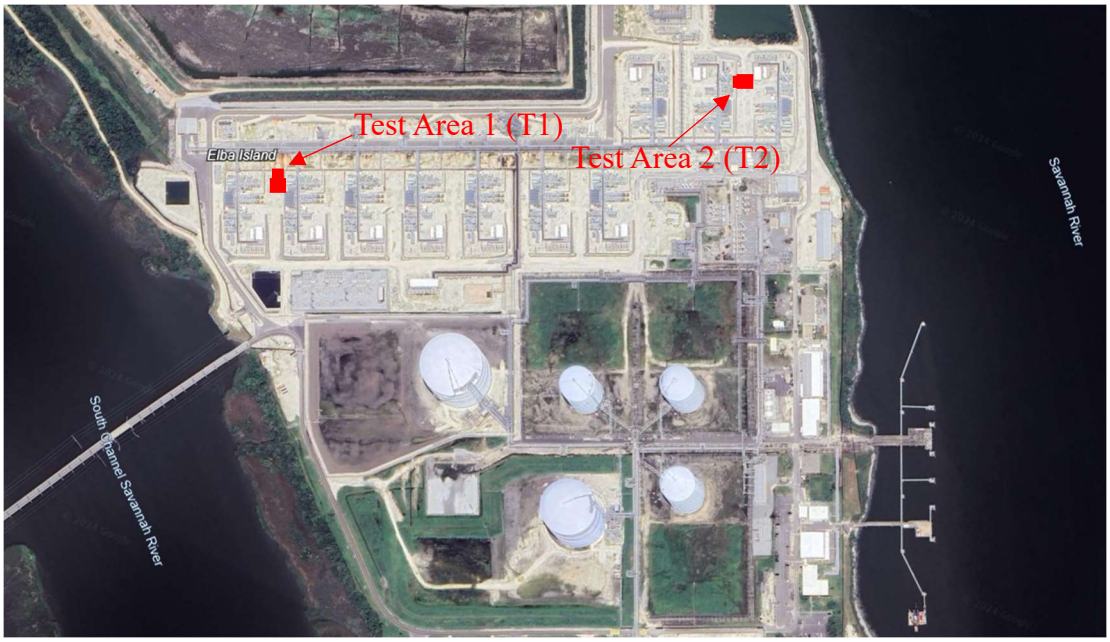

Source: Google Earth

Fig. 2-3. Test area layout

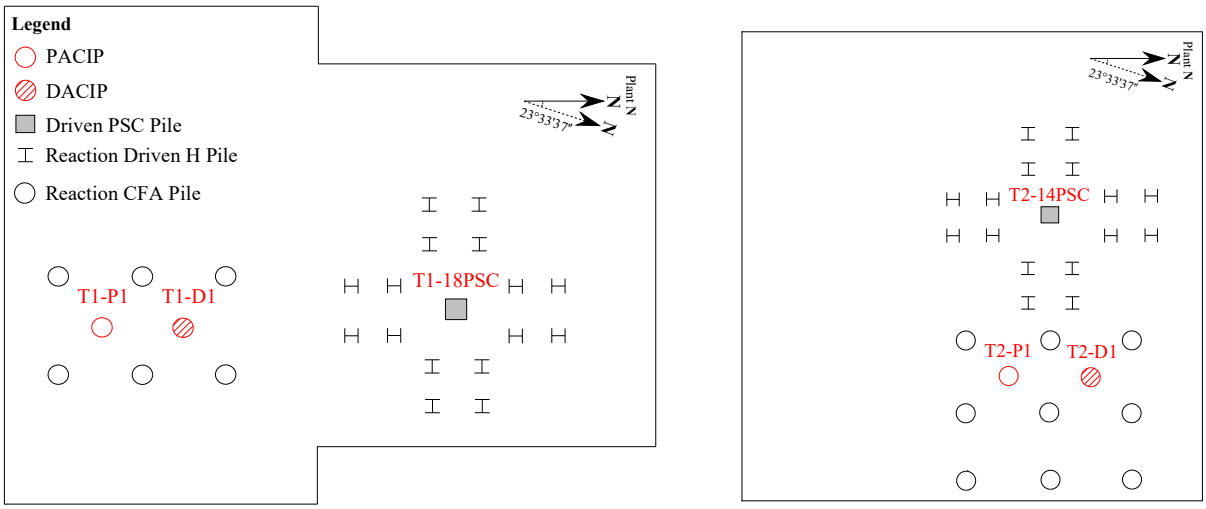

(a) (b)

Fig. 2-4. Test pile layout in test areas 1 and 2: (a) T1; (b) T2

Table 2-1. Information of test piles

Test Area	Test Piles	Pile Type*	Pile Diameter or Width (m)	Pile Length (m)	Pile Embedment (m)
T1	T1-18PSC	PSC	0.46	25.0	24.4
	T1-D1	DACIP	0.46	24.5	24.4
	T1-P1	PACIP	0.46	24.5	24.4
T2	T2-14PSC	PSC	0.36	20.4	18.6
	T2-D1	DACIP	0.46	20.0	19.8
	T2-P1	PACIP	0.46	20.0	19.8

*PSC = precast prestressed concrete; DACIP = full displacement augered cast in place; PACIP = partial displacement augered cast in place.

2.3.1 Pile instrumentation

The instruments for the test piles generally included the linear vibrating displacement transducers (LVDTs), load cells, and vibrating wire strain gages (VWSGs). For each test pile, four LVDTs were installed to measure pile head movement, a load cell mounted to the pile head was used to measure the head load, and VWSGs were attached to rebars in the piles to measure the axial strain during the mechanical loading. Figs. 2-5 (a) and 2-5 (b) illustrate the locations of VVSGs in the test piles in the two test areas. In general, each PSC was instrumented with a total of eight pairs of the strain gages. For each PACIP pile, five pairs of strain gages were attached the steel cages, which were only embedded to 2/3 of the pile length and the lower three single strain gages were attached the center bar, which was extended to the pile toe. The center bar was included to allow for the tensile load testing. For the DACIP, the one in test area 1 was only instrumented with single strain gages at eight depths, while the arrangement of the DACIP pile in test area 2 was similar to that of the PACIP piles.

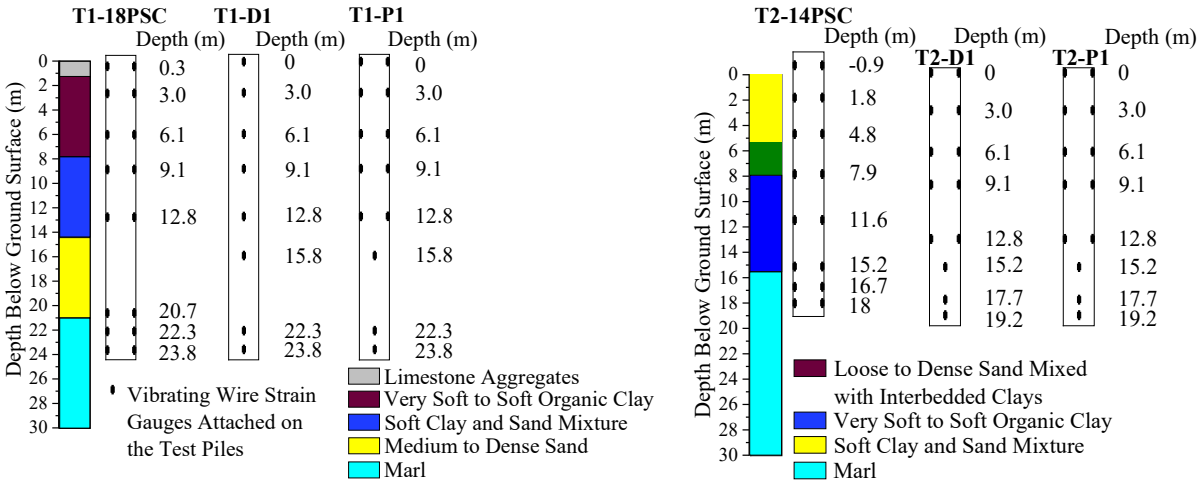

(a) (b)

Fig. 2-5. Instrumentation details for piles at test areas 1 and 2: (a) T1, and (b) T2

2.3.2 Pile load tests

A robust reaction frame was constructed to provide the necessary resistance against the applied loads. The frame was anchored securely to the ground using reaction piles, specifically groups of 14x89 HP reaction piles temporarily installed around the test pile and removed after the completion of the tests. Piles were spaced at least 2.4 m (i.e., 8 feet) in a clear distance in accordance with ASTM D1143-07 to minimize the interactions between reaction piles and test piles. Hydraulic jacks were used to apply static loads to the test piles, capable of applying compression loads. These jacks were positioned directly above the test piles to ensure vertical load application.

Static axial compressive load tests were performed in general accordance with ASTM D1143-07 using modified maintained load procedures. The load schedule for the pile load tests was designed to systematically apply and remove loads to measure the pile behavior under different conditions accurately. The loading procedure included multiple cycles of loading and unloading,

as well as a creep test to observe the time-dependent behavior of the piles. The load was incrementally applied to the pile in steps of 25% of the design load until the load reached 100% of the design load. At each increment, the load was held for one hour to allow the pile to reach equilibrium. When the load reached 100% of the design load, it was maintained for 12 hours. This period allowed for the observation of any time-dependent deformations or ‘‘creep’’ in the pile under sustained loading. Following the creep test, the load was further increased in steps of 50% of the design load until the load reached 250% of the design load or the failure of the pile, whichever occurs first. During this stage, each increment was again held for one hour. Afterwards, the pile was unloaded in a decrement of 50% of the design load to zero load. The holding time for each decrement was half an hour to allow the pile to stabilize at each load level.

2.4 Load test results

As discussed previously, piles in test area 2 were better instrumented than those in test area 1 (Fig. 2-5) and as will be discussed later, the results of piles in test area 2 contained a complete range of response. Therefore, this section only presents the load test results from test area 2, while those from test area 1 will be used as an independent set of data for verifying the proposed methods.

2.4.1 Pile installation in test area 2

Prior to the installation of T2-14PSC pile, a pilot hole to a depth of approximately 8.5 m was predrilled using a “baffle beam” (i.e., a 14-inch or 0.36-m H-pile with inclined steel plates welded between flanges near the HP pile toe) in order to hold the pile in position. An APE D19-42 open ended diesel hammer, with a ram weight of 4.2 kips (18.2 kN) and a maximum rated energy of 47.3 kip-feet (64.1 kN-m), was used to drive the test pile. During the driving of the test PSC pile,

hammer blow counts were recorded at each 0.3 m increment. The variation of hammer blow counts versus depth when installing T2-14PSC is illustrated in Fig. 2-6. The blow counts started at a depth of 8.5 m because of the predrilling as described above.

In general, the driving conditions varied significantly across different soil layers. The T2-14PSC pile was predrilled to a depth of 8.5 m. The initial driving through the soft clay and sand mixture required lower hammer blow counts, indicating less resistance and easier driving. However, as the pile penetrated deeper into the transition zone between the soft clay and sand mixture and the marl, the blow counts began to rise, reflecting the transition to a denser soil layer and corresponding higher resistance. The most challenging driving was encountered when the pile went deeper into the marl layer, where blow counts ranged from approximately 80 to 130 blows per 0.3 m. This significant increase in driving resistance highlights the considerable stiffness and density of the marl, which required more effort to penetrate. The pile driving analyzer tests were also performed during the driving, which indicated that the driving induced compressive and tensile stresses in the test pile were within the allowable limit.

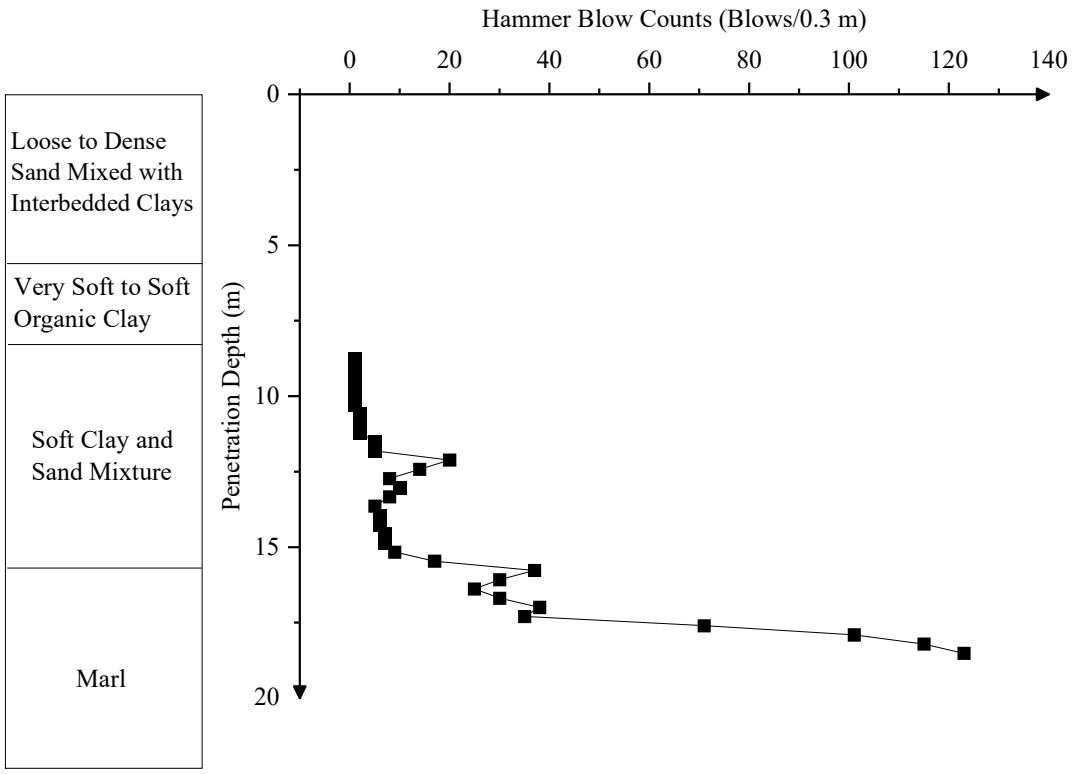

Fig. 2-6. Variation of hammer blow counts with pile penetration depths

Fig. 2-7 shows the installation record for the full displacement flight auger cast-in-place pile T2-D1. The installation was executed using a BG28 drilling rig, with the process involving approximately 17 minutes from start to completion. The key parameters recorded include penetration rate, hydraulic pressure applied to the tooling (i.e., the turntable that drives the auger's rotation), and grout pressure.

In general, an increase in penetration rate corresponded to a decrease in hydraulic pressure applied to the tooling. Grout pressure is observed between 12 and 16 minutes, corresponding to the moment when the auger has reached the designed depth and begins withdrawing. Overall, there was no difficulty in installing both DACIP and PACIP piles in this test area. The corresponding grout factor (actual grout volume divided by theoretical grout volume for borehole) was 1.56 and

1.39, respectively, which means the actual average diameter of the piles along embedment length was 25% and 18% greater than the original diameter of 0.46 m.

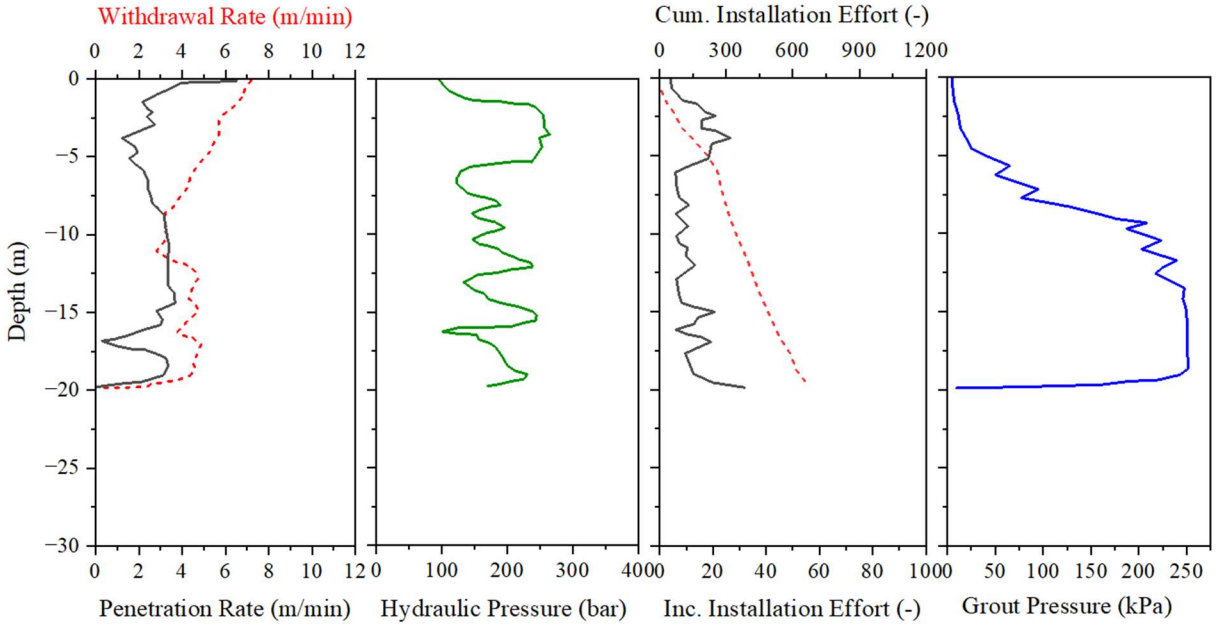

Fig. 2-7. Penetration rate, hydraulic pressure, installation effort, and grout pressure during installation of T2-D1

2.4.2 Compressive load test results from test area 2

One of the purposes of installing strain gauges at various depths along the pile was to determine the pile modulus. In this study, the tangent modulus method (Fellenius, 2001) was adopted, which requires full mobilization of the shaft resistance and utilizes the data from the strain gages at all positions (Lam and Jefferis, 2011). Fellenius (2009) suggests that the strain at all levels be in excess of 500 $\mu\varepsilon$ so that the test load is able to mobilize more than half of the strength of the pile material. This method assumes that the stress-strain of concrete is a second order polynomial. When the soils around the pile are mobilized at the ultimate loads, the tangent modulus versus strain curves measured at different strain gage levels would converge towards a constant line as shown in Fig.

2-8 for T2-D1. The same approach applied to the determination of pile modulus for other piles. The determined moduli of the test piles are shown in Table 2-2, which were used for interpretation of pile load test results as well as an input parameter in the numerical models to simulate the pile behavior under axial loading.

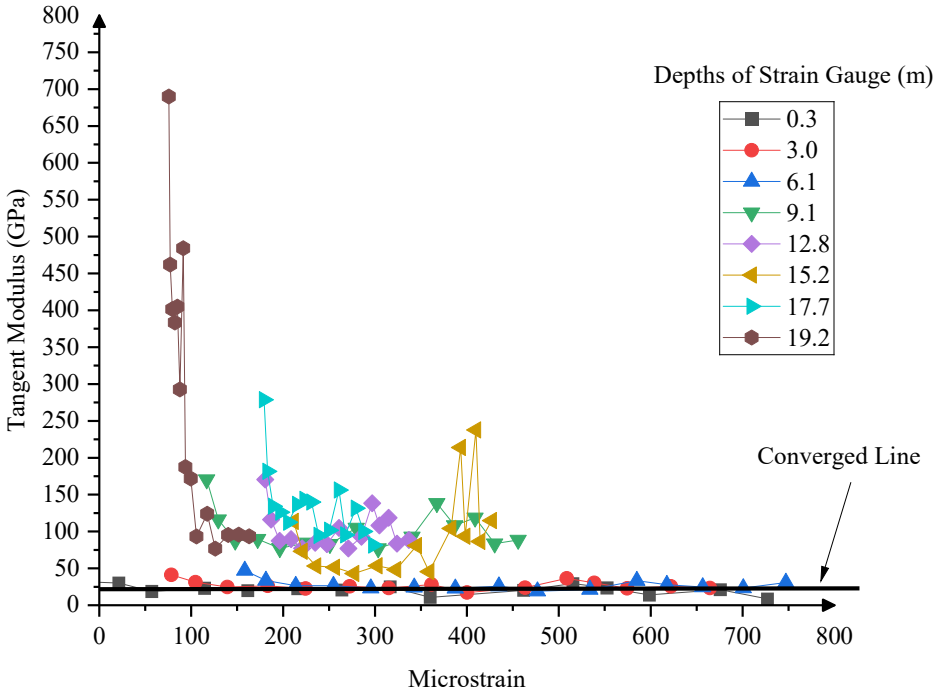

Fig. 2-8. Determination of tangent modulus (T2-D1)

Table 2-2. Tangent modulus of test piles (GPa)

Test Area 1	T1-18PSC	T1-D1	T1-P1
	37.9	28.7	25.4
Test Area 2	T2-14PSC	T2-D1	T2-P1
	36.8	23.5	28.7

The load-settlement curves for pile load tests of T2-14PSC, T2-D1, and T2-P1 are shown in Fig. 2-9. All three piles exhibit similar shapes of head load-displacement curves, with noticeable plunging failure. The ultimate load defined as the applied head loads at the onset of plunge was

greatest for T2-D1, followed by T2-P1, and T2-14PSC. However, the direct comparison of the ultimate loads between the three test piles is meaningless owning to the difference in pile diameter or side width and the varying levels of densification by the construction means. For example, T2-14PSC has a side wide of 14 inches (0.36 m) while the actual average diameter for T2-D1 and T2-P1 was 25% and 18%, respectively, greater than the originally designed diameter of 18 inches (0.46 m). The DACIP pile (T2-D1) tended to have a greater densification effect on surrounding soils than the PACIP pile (T2-P1). The head displacement (or settlement) leading to the onset of plunge was observed to be 9 mm, 13 mm, and 42 mm for T2-14PSC, T2-P1, and T2-D1, respectively. This variation in displacement might be affected by differences in pile modulus as shown in Table 2-2, but it is more likely associated with differences in pile side width or average diameter. A larger average pile diameter or side width engages a greater amount of soils near pile shaft or toe, mobilizing larger displacements to initiate the plunge.

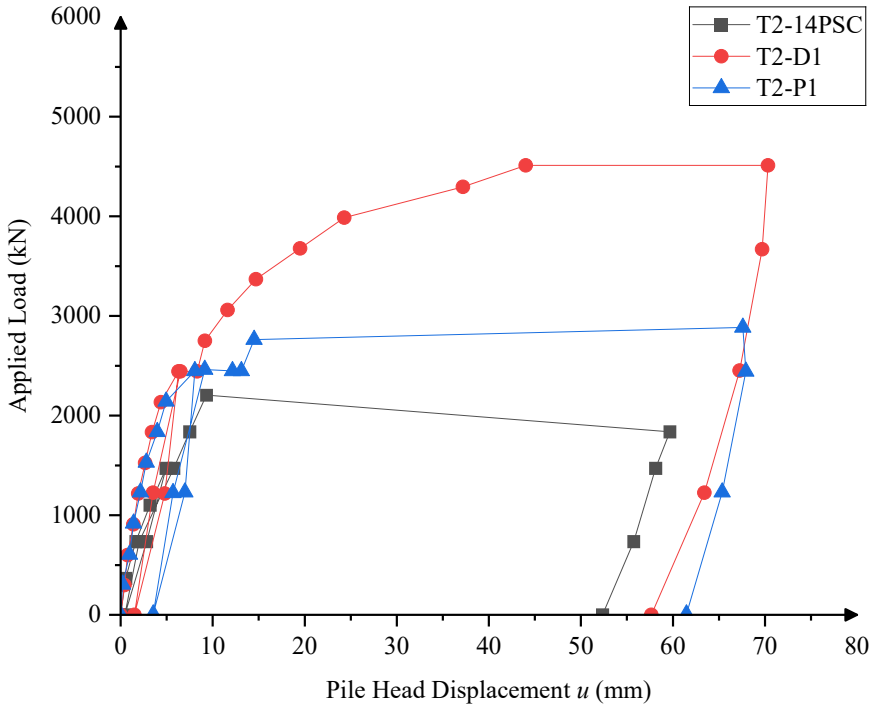

Fig. 2-9. Load-displacement curves for pile load tests

The axial force distributions for the three test piles in Fig. 2-10 reveal distinct load transfer behaviors. Both T2-14PSC and T2-P1 show a consistent decrease in the axial force with depth, reflecting typical load transfer through shaft friction and toe bearing. It is also evident that the axial force profiles for T2-D1 appeared a zigzag shape at a depth of 15 m, which indicated an enlarged pile cross section. The thermal integrity profiling (TIP) conducted for T2-D1 also confirmed the bulging at this depth, a transition from soft clay layer to a deeper stiff marl layer.

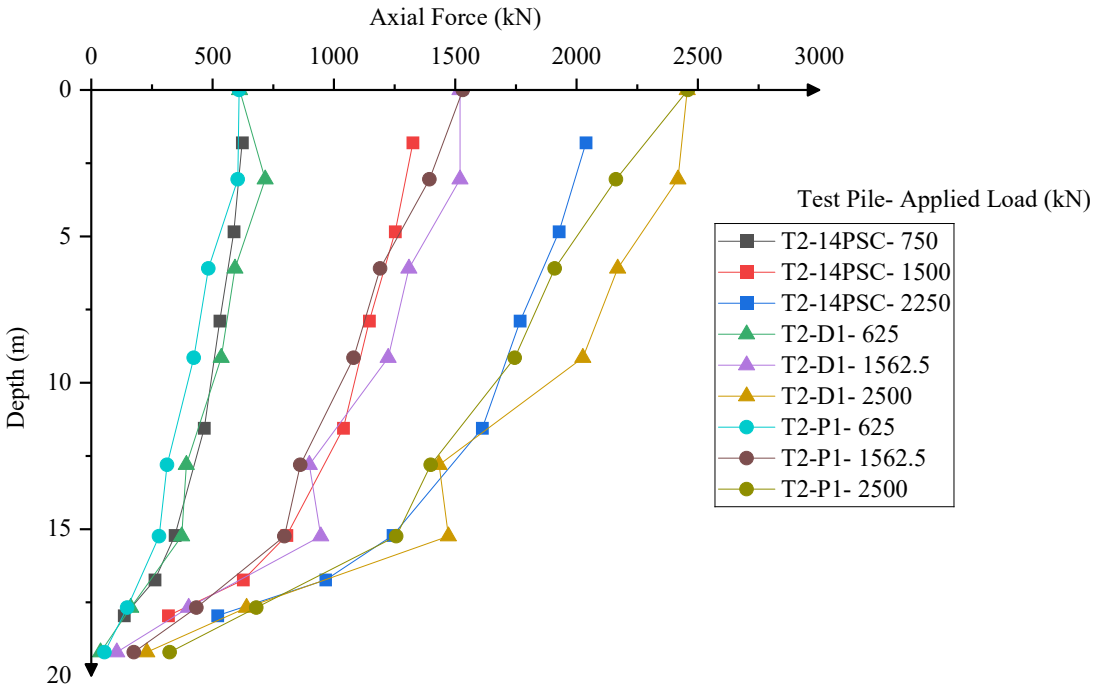

Fig. 2-10. Axial force distributions for pile load tests

2.4.3 CPT-based pile resistance prediction

The LCPC Method, developed by Bustamante and Gianeselli (1982), is a widely recognized approach for estimating shaft resistance and toe resistance directly from Cone Penetration Test (CPT) data. It is particularly favored for its simplicity and ease of application, as it directly relates the measured cone resistance to the pile resistance. This method involves calculating the ultimate

shaft resistance (f_s) and toe resistance (q_t) of piles using empirical correlations derived from extensive field data as shown in Eqs. (2-1) and (2-2).

$$f_s = q_c K_s \leq f_{sm} \quad (2\text{-}1)$$

$$q_t = q_{ca} K_t \quad (2\text{-}2)$$

where q_c = uncorrected CPT tip resistance; K_s = empirical correlation coefficient for shaft resistance (dimensionless); f_{sm} = the upper limit of f_s; q_{ca} = the average value of CPT q_c from below to above 1.5B relative to the pile toe, where B is pile side width or diameter; K_t = empirical correlation coefficient for toe resistance (dimensionless). For the stiff marl at the project site with CPT q_c = 5-10 MPa, the values of K_s, f_{sm}, and K_t, for PSC piles are taken as 0.0167, 35 kPa, and 0.55, respectively. Unfortunately, the LCPC method does not provide the values for DACIP piles or PACIP piles, but only for the augered cast in place (ACIP) piles. The corresponding values are 0.0167, 35 kPa, and 0.45, respectively. The LCPC method seems to only account for the effect of the construction means on the toe resistance while treating the driven and CFA piles equally for shaft resistance. From this perspective, DACIP and PACIP piles can take the same K_s and f_{sm} as PSC piles as the installation of these two piles would displace soils equal to or less than that of PSC piles. The values of K_t for DACIP piles may be taken as the same value for PSC piles (i.e., 0.55) while those for PACIP piles may be taken as the average of the values for ACIP and PSC piles (i.e., 0.5).

The Eslami and Fellenius Method is a direct CPT method that leverages CPT with pore pressure measurement (CPTu) data. This method, introduced by Eslami and Fellenius (1997), aims to enhance predictive accuracy by incorporating both cone resistance and pore pressure measurements, which offer a more comprehensive understanding of soil behavior. The method

calculates the ultimate shaft resistance and toe resistance using empirical equations that factor in cone resistance and pore pressure parameters as shown in Eqs. (2-3) and (2-4).

$$f_s = q_E C_s \tag{2-3}$$

$$q_t = q_{Eg} C_t \tag{2-4}$$

where q_E = cone resistance after correction for pore pressure on the cone shoulder and adjustment to apparent "effective" stress; $q_E = q_T - U_2$, in which q_T is the cone resistance corrected for porewater and net area ratio effects; C_s = empirical correlation coefficient for shaft resistance (dimensionless); q_{Eg} = the geometric average of the q_E over the influence zone which is suggested to be taken as $2B$ above the pile tip and $4B$ below the pile tip by Eslami and Fellenius (1997); C_t = empirical correlation coefficient for toe resistance (dimensionless). The authors provided the range and suggested approximation values of C_s for five main soil categories of the soil profiling diagram including soft sensitive soils, clay, stiff clay and mixture of clay and silt, mixture of silt and sand, and sand. Unfortunately, there is no data specifically for marl. The suggested value for stiff clay and mixture of clay and silt is 0.025 which will be used for the evaluation of the accuracy and applicability of this method in marl in next section. For C_t, a value of 1.0 is recommended.

Tables 2-3 and 2-4 show the predicted shaft resistance (f_s) and toe resistance (q_t) of pile in the marl, respectively, using the LCPC and Eslami and Fellenius methods as well as the measured values from the static load tests in test area 2. The results reveal that the LCPC method significantly underestimates both shaft and toe resistances for piles in marl, aligning with the findings of Tan and Lin (2011). The errors of underestimation were more considerable for the shaft resistance (at a range of 77.0% to 86.2%) than the toe resistance (at a range of 15.5% to 23.2%). Several limitations of the LCPC method contribute to this disparity: a) it is primarily developed based on full-scale bored piles rather than driven piles; b) it disregards the pore pressure acting on the CPT

cone shoulder; c) it uses the vertical total stress instead of the vertical effective stress, which governs the long-term behavior of the pile; d) it imposes unjustified upper limits on the unit shaft resistance (35 kPa for stiff clay).

In contrast, the Eslami and Fellenius method provides relatively more accurate predictions than the LCPC method in terms of shaft resistance. The errors of underestimation from this method were approximately in a range of 27.9 to 57.0% for the shaft resistance. However, the toe resistance was overestimated by up to 52.1%, which is unsafe. The above results indicated that both prevalent methods did not yield well prediction of pile resistance in stiff marl due to poorly correlative coefficients (K_s and K_t for the LCPC as well as C_s and C_t for the Eslami and Fellenius method) or unjustified upper limits. Therefore, it is necessary to propose better correlations specifically for piles in stiff mark.

Table 2-3. Predicted and measured shaft resistance (f_s)

Pile	Measured f_s (kPa)	LCPC		Eslami and Fellenius	
		Predicted f_s (kPa)	Error (%)	Predicted f_s (kPa)	Error (%)
T2-P1	152.0	35.0	-77.0	109.5	-27.9
T2-D1	195.3	35.0	-82.1	109.5	-43.9
T2-14PSC	253.9	35.0	-86.2	109.2	-57.0

Table 2-4. Predicted and measured toe resistance (q_t)

Pile	Measured q_t (kPa)	LCPC		Eslami and Fellenius	
		Predicted q_t (kPa)	Error (%)	Predicted q_t (kPa)	Error (%)
T2-P1	3170.6	2678.1	-15.5	4821.1	52.1
T2-D1	3565.8	2945.9	-17.4	4821.1	35.2
T2-14PSC	4015.2	3082.1	-23.2	4340.1	8.1

2.4.4 Improved resistance prediction for driven and CFA piles in stiff marl

Based on the load tests from test area 2, the improved correlative coefficients for shaft and toe resistance are suggested in Tables 2-5 and 2-6. These improved coefficients were back calculated involves using CPT data and pile load test results, and for the LCPC method, the forced upper bound of the ultimate shaft resistance (f_{sm}) is removed.

Table 2-5. Suggested coefficients for piles in stiff marl for the LCPC method

Type	Pile	Coefficient for shaft resistance *Ks*	Coefficient for toe resistance *Kt*
PACIP	T2-P1	0.027 (0.0167)	0.592 (0.50)
DACIP	T2-D1	0.034 (0.0167)	0.666 (0.55)
Driven	T2-14PSC	0.044 (0.0167)	0.717 (0.55)

Note: Values inside the brackets are those either suggested in the original methods or recommended by the authors.

Table 2-6. Suggested coefficients for piles in stiff marl for the Eslami and Fellenius method

Type	Pile	Coefficient for shaft resistance C_s	Coefficient for toe resistance C_t
PACIP	T2-P1	0.035 (0.025)	0.658 (1.0)
DACIP	T2-D1	0.045 (0.025)	0.740 (1.0)
Driven	T2-14PSC	0.058 (0.025)	0.925 (1.0)

Note: Values inside the brackets are those either suggested in the original methods or recommended by the authors.

The improved correlations for shaft and toe resistances using the LCPC and Eslami and Fellenius method were verified with additional pile load tests. The verification was conducted on three test piles: T1-P1, T1-D1, and T1-18PSC. The results are summarized in Tables 2-7 and 2-8. The comparison for the full displacement flight auger cast-in-place pile has been omitted as the available pile load test data could not reach the ultimate capacity due to limitations in the testing equipment, making it unsuitable for rigorous verification.

Table 2-7. Verification results of shaft resistance

Type	Pile	Measured f_s (kPa)	LCPC		Eslami and Fellenius	
			Predicted f_s (kPa)	Error (%)	Predicted f_s (kPa)	Error (%)
PACIP	T1-P1	175.7	188.3	7.2	164.6	-6.3
Driven	T1-18PSC	290.9	310.4	6.7	275.7	-5.2

Note: The comparison for the full displacement flight auger cast-in-place pile has been excluded because the available pile load test data did not reach ultimate capacity due to limitations in the load testing equipment.

Table 2-8. Verification results of toe resistance

Type	Pile	Measured q_t (kPa)	LCPC		Eslami and Fellenius	
			Predicted q_t (kPa)	Error (%)	Predicted q_t (kPa)	Error (%)
PACIP	T1-P1	4748.1	4098.6	-13.7	3051.0	-35.7
Driven	T1-18PSC	4766.9	4961.2	4.1	4292.0	-10.0

Note: The comparison for the full displacement flight auger cast-in-place pile has been excluded because the available pile load test data did not reach ultimate capacity due to limitations in the load testing equipment.

The verification reveals several key points. For shaft resistance (f_s), the LCPC method with adjusted coefficients generally provides a reasonable prediction. The discrepancies between the predicted and measured shaft resistances for PACIP was relatively small, at 7.2%, indicating the method's effectiveness in estimating shaft resistance for this pile type with minor overestimations. For driven piles, the error was smaller at 6.7%. However, the predictions for toe resistance (q_t) showed some variability. For the PACIP and driven piles, T1-P1 and T1-18PSC, the errors were -13.7% and 4.1%, respectively, indicating both underestimations and overestimations depending on the pile type.

The Eslami and Fellenius method with adjusted coefficients generally provides a reasonable approximation for pile-soil interface resistance. The differences between the predicted and measured shaft resistances (f_s) for PACIP and driven pile were found to be small, at -6.3% and -5.2%. The predictions for toe resistance (q_t) using the Eslami and Fellenius method showed

difference with measured data from pile load test ranged from -35.7% to -10.0%. Notably, underestimation occurred across all pile types and remained within an acceptable range, which is ideal for design purposes.

Overall, both of the improved CPT-based pile resistance prediction methods are relatively reliable, showing reduced error in verification. However, there remains a tendency for slight overestimation, which is undesirable in design. Therefore, further improvements to the current predictions are necessary. First, to minimize potential errors in the improved coefficients, it is necessary to utilize multiple CPT results from within a test area (when available) for the back-calculation of coefficients and to compare the differences among them. While marl is generally more consistent than other soil layers at this site, variability still exists. Relying on limited CPT points (e.g., one CPT per test area) can overlook spatial variations and localized anomalies, leading to incomplete or inaccurate representations of soil behavior. Second, incorporating more pile load test data for each type of pile into the database can help reduce biases introduced by testing devices, operating practices, and other factors.

2.5 Numerical analyses of axially loaded driven and displacement CFA piles

For piles under axial loading, the pile responses can be simply computed by considering piles as a column supported by a series of Winkler's types of nonlinear springs along the pile shaft and at the pile toe. The springs supporting the shaft are defined by *t-z* curves while those supporting the pile toe by *Q-z* curves. The governing equation and boundary condition for this problem are given in Eqs. (2-5) and (2-6).

$$E_p \frac{d^2u}{dz^2} - \tau_s R_{ca} = 0 \tag{2-5}$$

$$\begin{cases} E_p A_p \frac{d^2u}{dz^2} = P_h \ \ for\ z = 0 \\ E_p A_p \frac{d^2u}{dz^2} = Q \ \ for\ z = L_p \end{cases} \tag{2-6}$$

where E_p = pile modulus; u = displacement of pile at a given depth, z; z = depth below pile head, with $z = 0$ representing pile head and $z = L_p$ representing pile toe; τ_s = shaft reaction at a given depth, z (e.g., in kPa) and $\tau_s \leq f_s$; R_{ca} = a ratio of pile circumference to cross-sectional area (e.g., m^{-1}); A_p = cross-sectional area of pile; P_h = load applied at the pile head; Q = toe reaction provided by soil (in kN); L_p = pile length.

In Eq. (2-5), shaft reaction is a function of pile displacement, which typically appears in a nonlinear relationship, commonly known as "*t-z*" curves (equivalent to τ_s-u curves in this paper). Similarly, there exists a nonlinear relationship between toe reaction and toe displacement, also known as "*Q-z*" curves, which are equivalent to Q-u_t curves in this paper. Among the existing relationships, the hyperbolic function has been most widely used to characterize both τ_s-u and Q-u_t curves (e.g., Lee and Xiao, 2001) for piles in different types of soils such as clays and sands. However, this model could not address the degradation of shaft reaction of the pile subjected to axial loading. This issue is resolved by Zhang and Zhang (2012), who propose a new function given in Eq. (2-7) to account for the softening responses of pile shaft; however, in their method the toe reaction is simply considered bilinear to the toe displacement to ease the numerical iteration, as given in Eq. (2-11). They further apply the method to driven piles and bored piles in soft clay, sands, and weak rock. Unfortunately, none of the existing methods directly takes into account driven piles or displacement CFA piles in stiff marl.

$$\tau_s = \frac{(a+c\,u)u}{(a+b\,u)^2} \tag{2-7}$$

$$a = (b - 2c)u_{su} = \frac{(\beta_s - 1 + \sqrt{1-\beta_s})u_{su}}{2\beta_s f_s} \tag{2-8}$$

$$b = \frac{1-\sqrt{1-\beta_s}}{2\beta_s f_s} \tag{2-9}$$

$$c = \frac{2-\beta_s-2\sqrt{1-\beta_s}}{4\beta_s f_s} \tag{2-10}$$

$$Q = \begin{cases} k_1 u_t & u_t \le u_{ty} \\ k_2(u_t - u_{ty}) + k_1 u_{ty} & u_t > u_{ty} \end{cases} \tag{2-11}$$

where a, b, and c are empirical coefficients; u = the relative displacement at the pile-soil interface at a specific depth; f_s = ultimate shaft resistance, i.e. the maximum value of τ_s; u_{su} = the displacement at the ultimate shaft resistance; β_s is the ratio of the residual shaft resistance to the ultimate shaft resistance; k_1 and k_2 are two slopes of the bilinear curve; Q = the pile toe resistance in kN; u_t = displacement at the pile toe-i.e., $u_t = u(L_p)$; u_{ty} = the yield displacement at pile toe.

2.5.1 Proposed "*t-z*" and "*Q-z*" relationships for piles in stiff marl

To advance the analysis for piles in stiff marl that exhibits distinct strain softening at both pile shaft and toe, this study proposes a new model based on Zhang and Zhang (2012) to interpret the load test results. The shaft reaction is calculated using the same "*t-z*" curves by Zhang and Zhang (2012): i.e., τ_s-u curves in this study, expressed in Eqs. (2-7)-(2-10). However, different from the bilinear "*Q-z*" curves (i.e., Q-u_t) by Zhang and Zhang (2012), the toe reaction in this study is also modelled as strain softening as given in Eq. (2-12) and illustrated in Fig. 2-11:

$$Q = \frac{u_t(a_t + c_t\, u_t)}{(a_t + b_t\, u_t)^2} \tag{2-12}$$

$$a_t = (b_t - 2c_t)u_{tu} \tag{2-13}$$

$$b_t = \frac{1-\sqrt{1-\beta_t}}{2\beta_t Q_u} \tag{2-14}$$

$$c_t = \frac{2-\beta_t-2\sqrt{1-\beta_t}}{4\beta_t Q_u} \tag{2-15}$$

where a_t, b_t, and c_t are empirical coefficients; Q_u = the ultimate pile toe resistance in kN; u_{tu} = the toe displacement corresponding to the ultimate toe resistance; β_t = the ratio of the residual toe resistance to the ultimate toe resistance.

Since τ_s and Q are nonlinearly related to the displacement u, a close-form solution for Eqs. (2-5) and (2-6) is impossible. Therefore, a finite difference procedure (i.e., central finite difference scheme) is applied to solve this nonlinear problem, mathematically given by Eqs. (2-5)-(2-10) and Eqs. (2-12)-(2-15). Furthermore, the Newton-Raphson method is adopted for the iterative calculation. A MATLAB code was developed to implement the finite difference procedure.

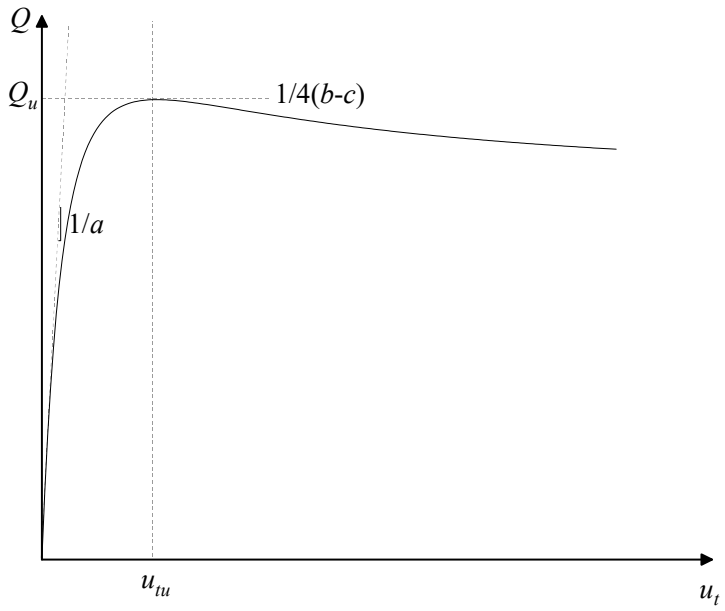

Fig. 2-11. The toe reaction-displacement (Q-u_t) curve for the pile toe in stiff marl

2.5.2 Determination of model parameters for piles in stiff marl

Some of the model parameters were determined through back-calculation using pile load tests in test area 2, in which the parameters are adjusted until the model output best fits the measured results from the pile load tests-i.e., pile head load-movement as well as axial load distribution. The

parameters involved in the proposed model include f_s, u_{su}, and β_s for shaft resistance as defined in Eqs. (2-5)-(2-10) and Q_u, u_{tu}, and β_t for toe resistance as defined in Eqs. (2-12)-(2-15). Among these parameters, f_s and Q_u can be estimated directly using the improved correlation suggested in Tables 2-5 and 2-6 while the other four parameters are calibrated based on the test results from the piles in test area 2. The reading from the first strain gauge of T2-14PSC is negligible since it is located above the ground.

Table 2-9 presents the determined and back-calculated model inputs for shaft and toe resistances for three different types of piles. These parameters include the ultimate shaft resistance (f_s), the displacement at ultimate shaft resistance (u_{su}), and the residual shaft resistance coefficient (β_s) for the pile shaft. For the pile toe, the parameters include the ultimate toe resistance (Q_u), the displacement at ultimate toe resistance (u_{tu}), and the residual toe resistance coefficient (β_t). The ultimate shaft and toe resistances (f_s and Q_u) can be calculated using CPT based correlations developed in previous section as mentioned above. The suggested displacements corresponding to the ultimate shaft and toe resistances (u_{su} and u_{tu}) are provided in Table 2-9, where driven piles and PACIP exhibit very similar u_{su} and u_{tu} values, while DACIP has significantly larger suggested values. The values of β_s and β_t are in a small range; Zhang et al. (2012) suggested values of β_s for bored piles range from 0.83 to 0.97. For this study, β_s and β_t are suggested to be 0.9 for both PACIP and driven piles, while for DACIP, it is slightly larger at 0.92.

Table 2-9. Input parameters for *t-z* and *Q-z* curves

Type	Pile	Shaft			Toe		
		f_s[1] (kPa)	u_{su}[2] (mm)	β_s[2]	Q_u[1] (kPa)	u_{tu}[2] (mm)	β_t[2]
PACIP	T2-P1	152.0	8.0	0.9	3170.6	6.0	0.9
DACIP	T2-D1	195.3	17.0	0.92	3565.8	17.0	0.92
Driven	T2-14PSC	253.9	9.0	0.9	4015.2	7.0	0.9

Note:
1. f_s and Q_u are determined using CPT based correlations developed in previous section.
2. u_{su}, β_s, u_{tu}, and β_t are back-calculated values.

Figs. 2-12 to 2-17 show the good fit of the simulated to the measured data in two sets of data involving head load-movement as well as load transfer along pile length. These figures demonstrate that the model can replicate the initial stiffness, peak load, and post-peak behavior of the pile. The simulation closely follows the test data with only minor deviations in most cases. The model accurately captures the load transfer mechanism, indicating the effectiveness of the calibrated parameters in representing the strain-softening behavior of marl.

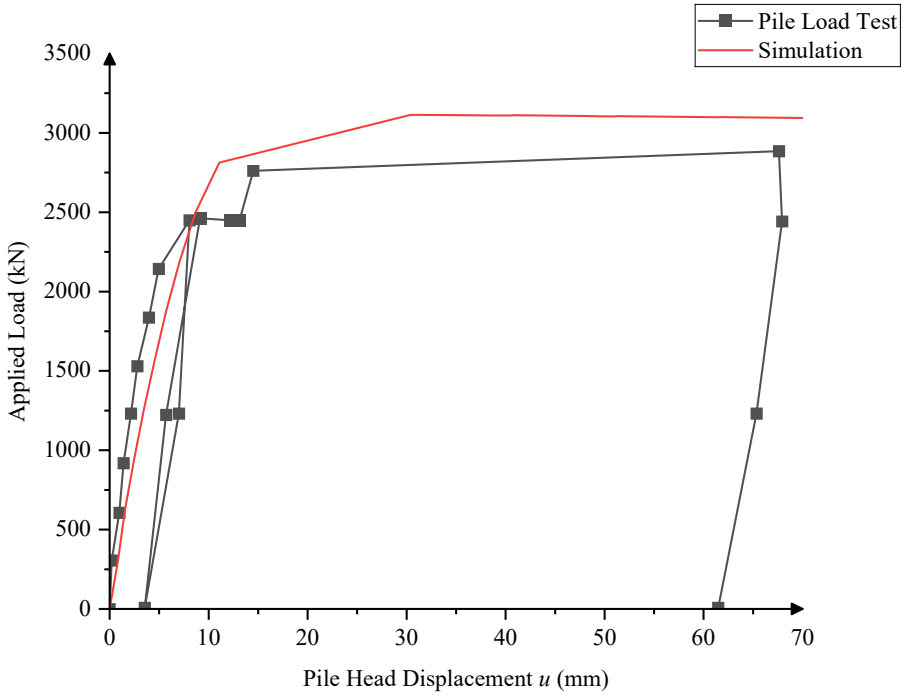

Fig. 2-12. Comparison of load-displacement curves between simulation and pile load test for T2-P1

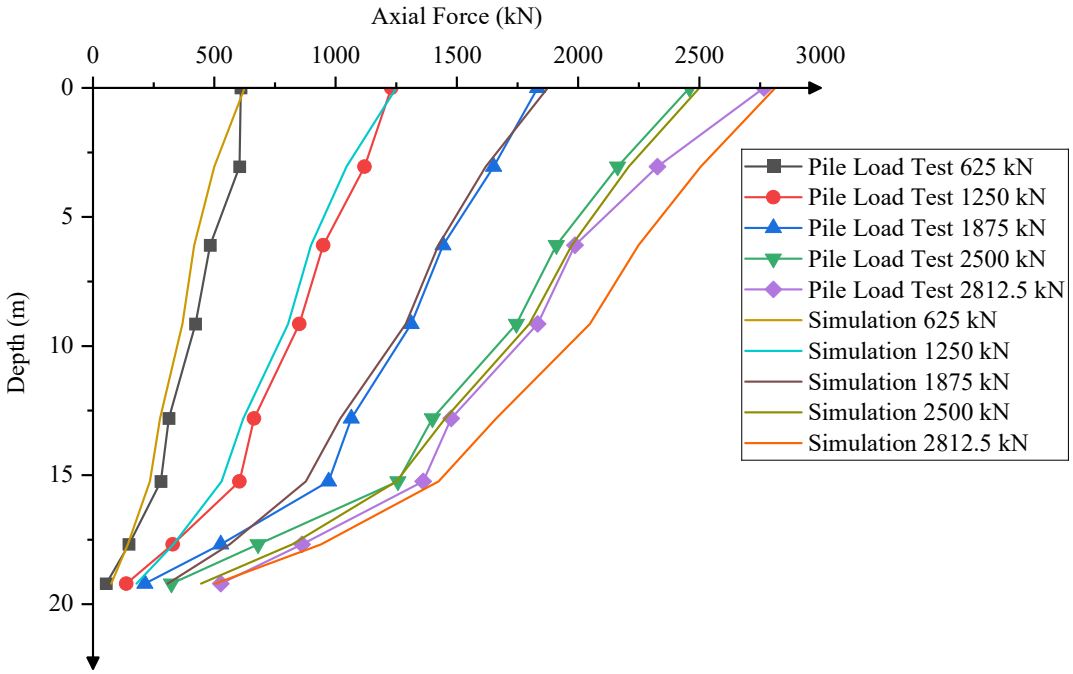

Fig. 2-13. Axial force distribution comparison at various load levels for T2-P1

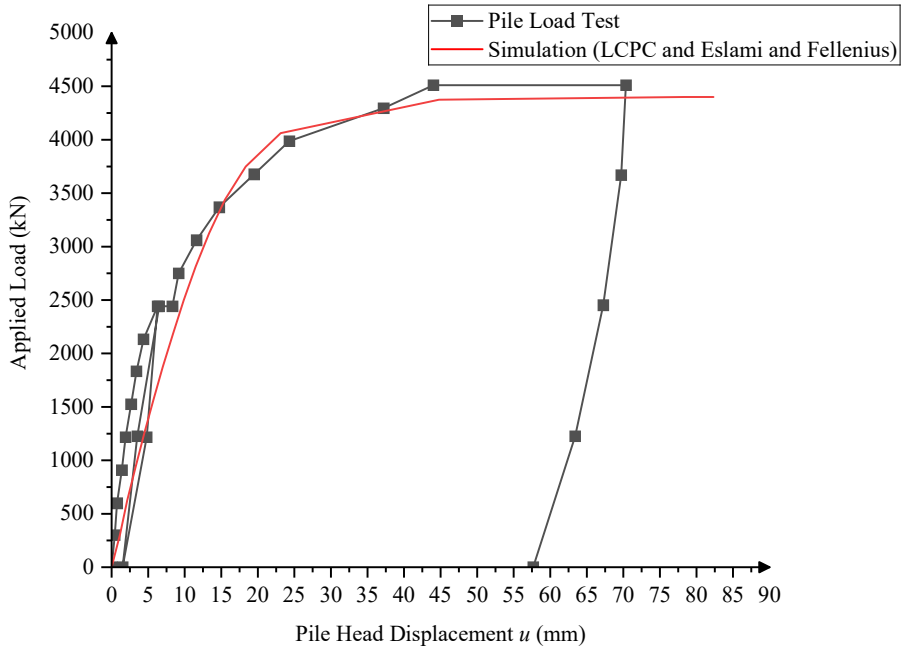

Fig. 2-14. Comparison of load-displacement curves between simulation and pile load test for T2-D1

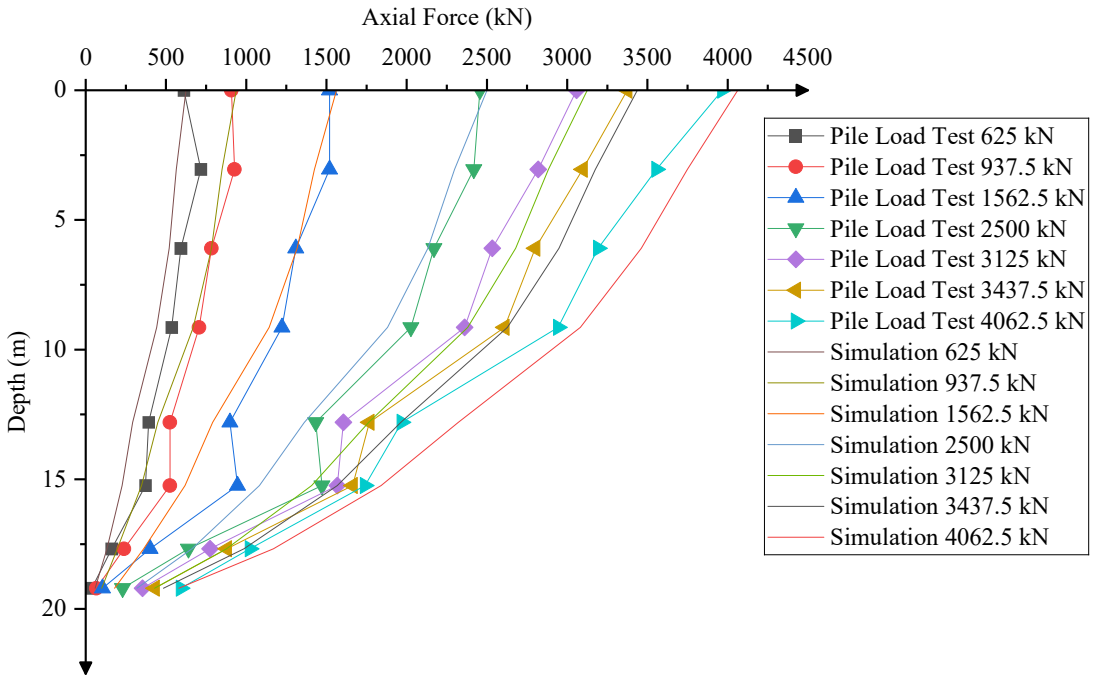

Fig. 2-15. Axial force distribution comparison at various load levels for T2-D1

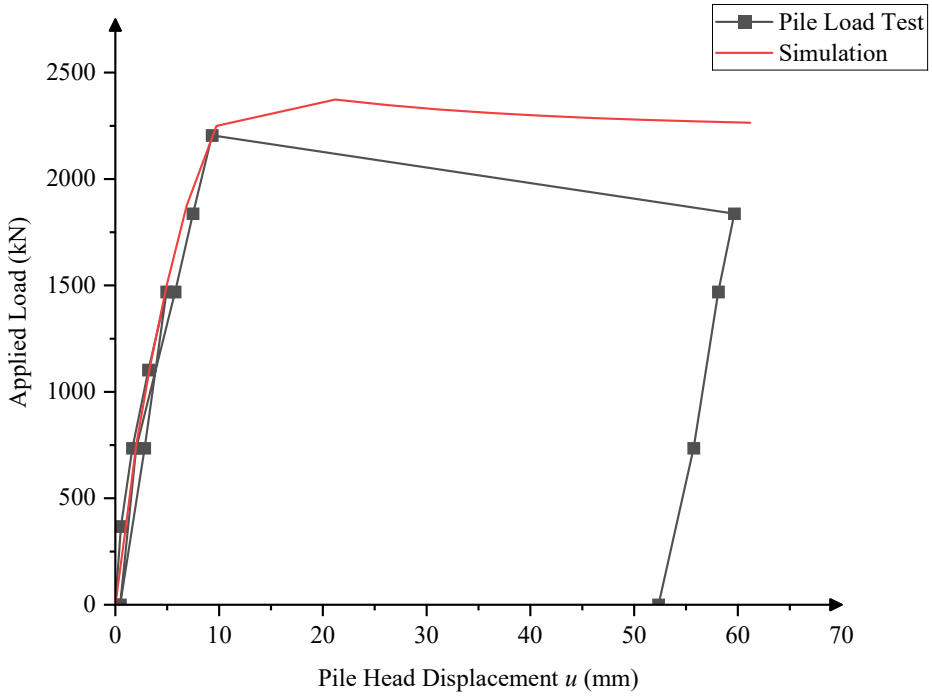

Fig. 2-16. Comparison of load-displacement curves between simulation and pile load test for T2-14PSC

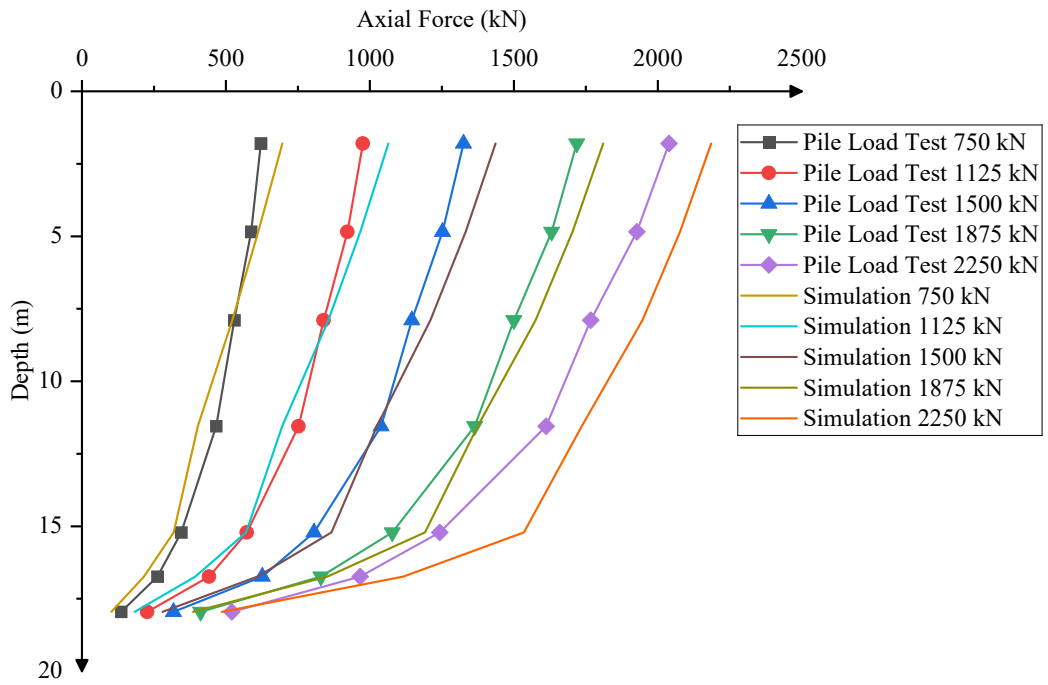

Fig. 2-17. Axial force distribution comparison at various load levels for T2-14PSC

2.5.3 Model verification

For the verification of the developed model and its correlations, three test piles were used: T1-P1, T1-D1, and T1-18PSC. T1-P1 is an 18-inch (i.e., 0.46 m) partial displacement CFA pile in Area 1. T1-D1 is an 18-inch (i.e., 0.46 m) full displacement CFA pile located in Area 1. T1-18PSC is a 18-inch (i.e., 0.46 m) precast prestressed concrete pile in Area 1. Verification of numerical model using CPT results and developed correlations

The model inputs f_s and Q_u were correlated using the LCPC and Eslami and Fellenius method, and the remaining inputs for the upper soil layers were adjusted to align the axial force distribution with the measured values from the pile load tests. Table 2-10 summarizes the model inputs used for the verification process:

Table 2-10. Model inputs for verification

Method	Type	Pile	Shaft			Toe		
			f_s (kPa)	u_{su} (mm)	β_s	Q_u (kPa)	u_{tu} (mm)	β_t
LCPC	PACIP	T1-P1	188.3	8	0.9	4098.6	6	0.9
	DACIP	T1-D1	241.9	17	0.92	4609.5	17	0.92
	Driven	T1-18PSC	310.4	9	0.9	4961.2	7	0.9
Eslami and Fellenius	PACIP	T1-P1	164.6	8	0.9	3051.0	6	0.9
	DACIP	T1-D1	211.5	17	0.92	3431.3	17	0.92
	Driven	T1-18PSC	275.7	9	0.9	4292.0	7	0.9

2.5.4 Analysis of verification results

In this section, we present the verification of the developed correlations for numerical model inputs using CPT data. The model inputs were calculated based on the correlations developed in the previous section, and the remaining inputs for the upper soil layers were adjusted to align the axial force distribution with the measured values from the pile load tests. The verification results are shown in Figs. 2-18 to 2-23.

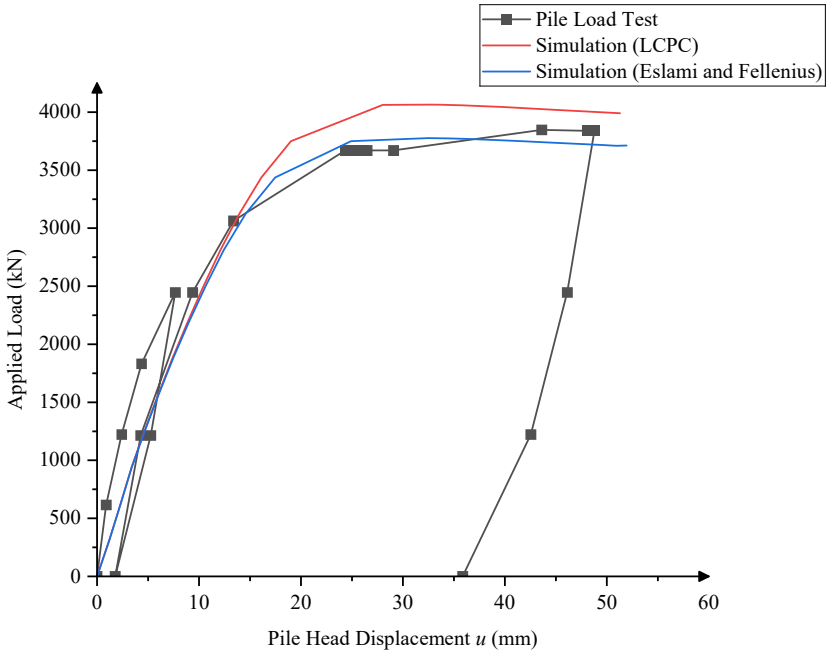

Fig. 2-18. Comparison of simulated and measured load-displacement curves for T1-P1

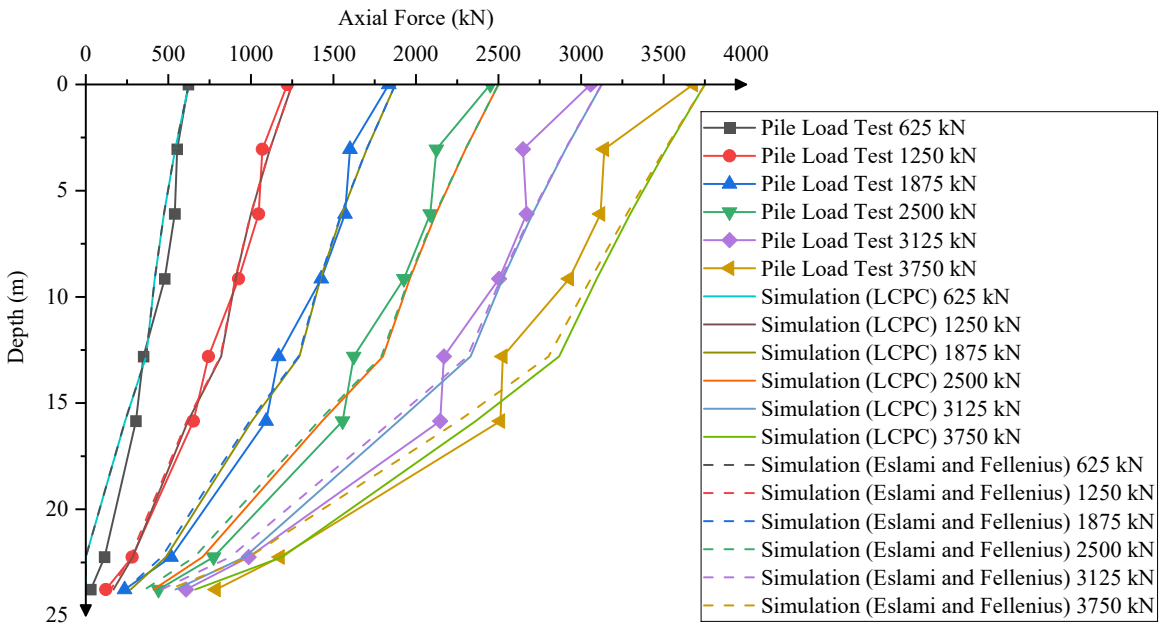

Fig. 2-19. Axial force distribution comparison at various load levels for T1-P1

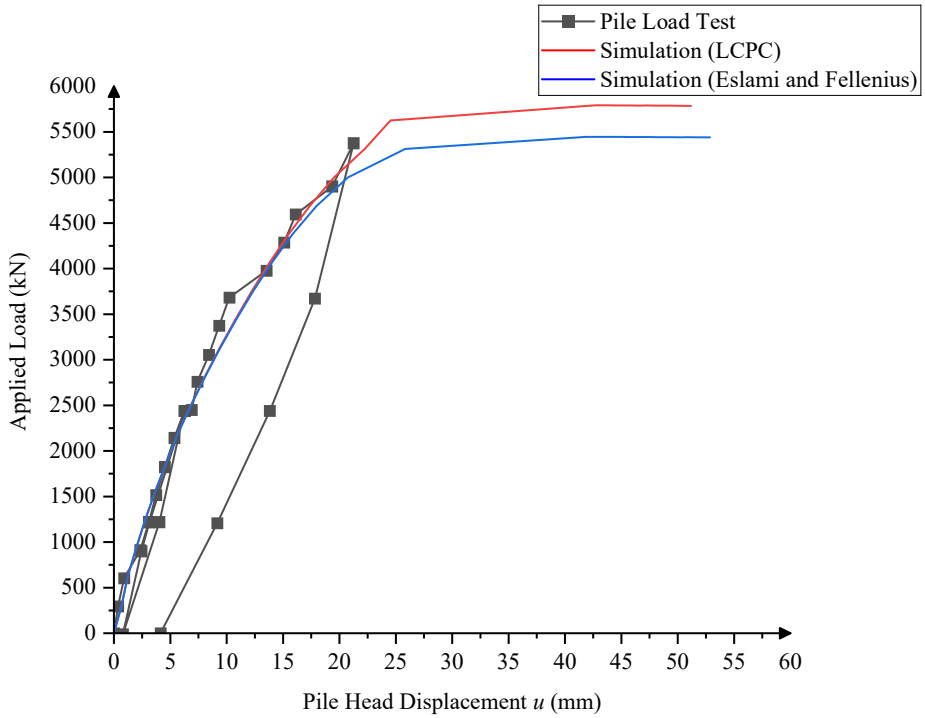

Fig. 2-20. Comparison of simulated and measured load-displacement curves for T1-D1

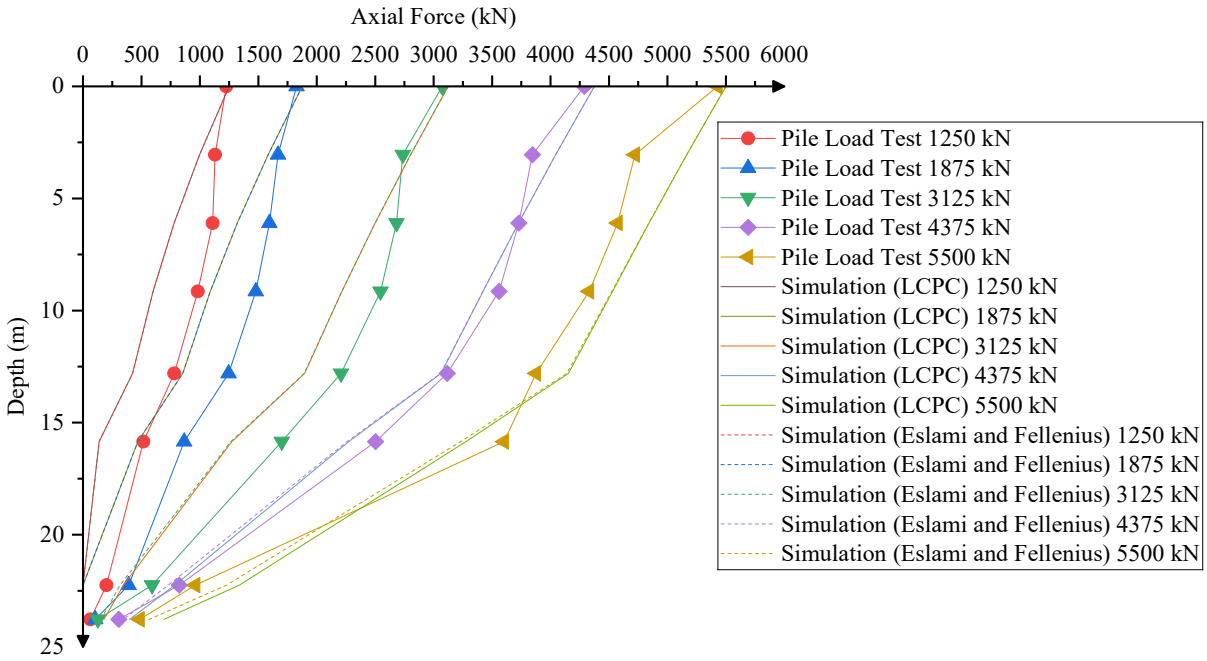

Fig. 2-21. Axial force distribution comparison at various load levels for T1-D1

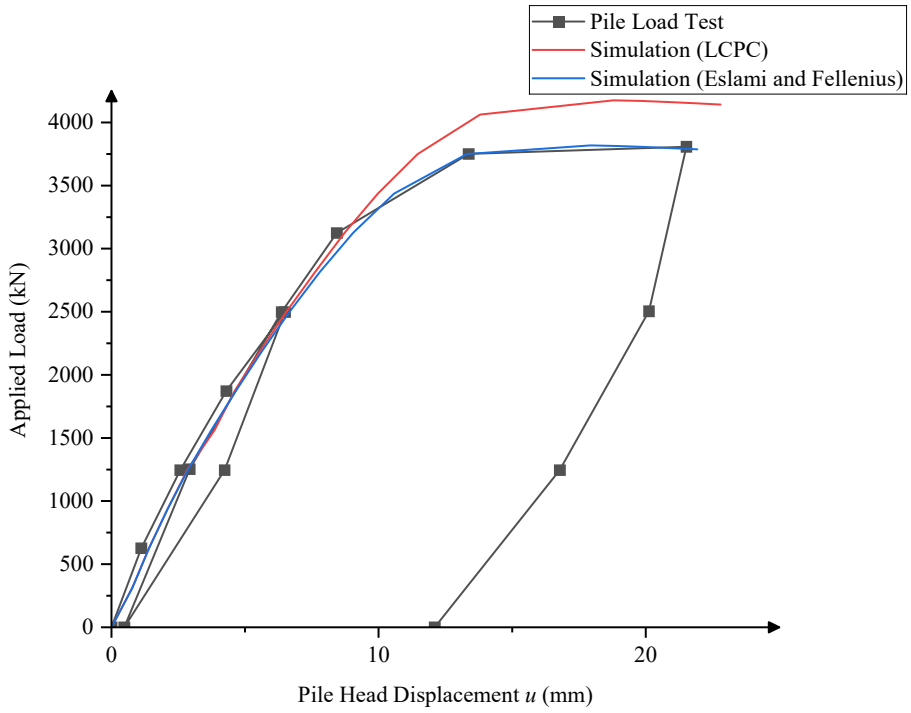

Fig. 2-22. Comparison of simulated and measured load-displacement curves for T1-18PSC

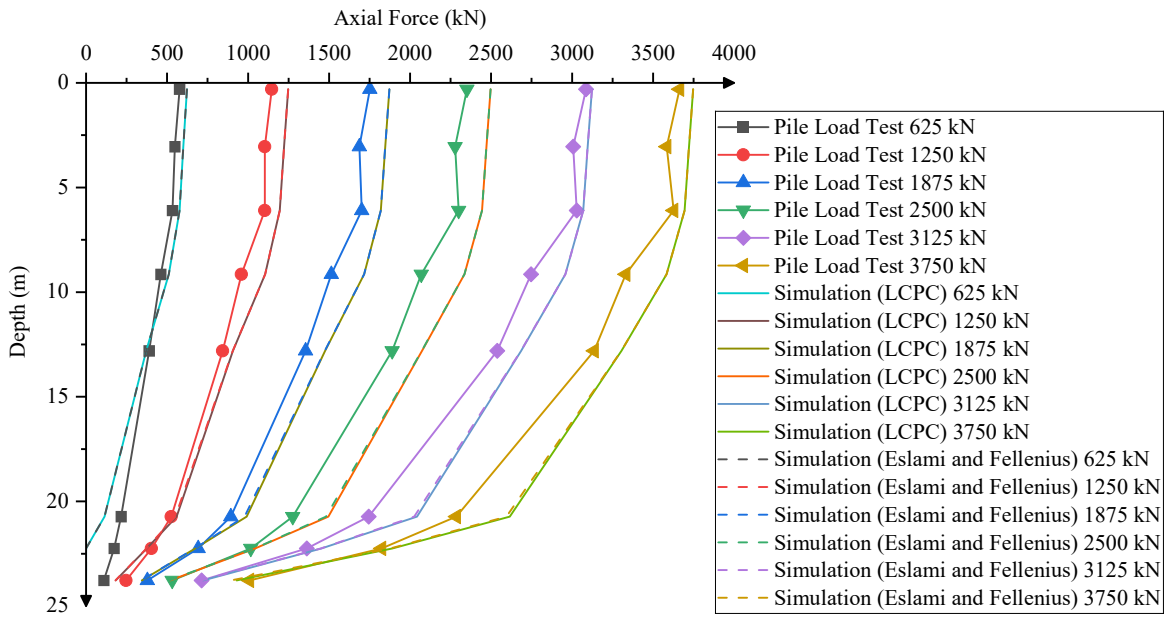

Fig. 2-23. Axial force distribution comparison at various load levels for T1-18PSC

For T1-P1, the Eslami and Fellenius method shows a closer match to the measured data, especially at higher displacements, indicating a more accurate prediction of ultimate capacity. In contrast, the LCPC method slightly overestimates the ultimate capacity. The axial force distribution shows that the simulation using the LCPC method aligns better than the Eslami and Fellenius method. Although both methods present certain discrepancies, the LCPC method fits more closely with the measured data in marl, particularly at higher loads at the pile toe.

For T1-D1, the pile load test was terminated at an early stage, so the pile was not loaded until failure, leaving the nonlinear part of the curve incomplete and making the ultimate capacity indeterminate from the test data alone. However, based on the trend of the load-displacement curve, where the slope of the tangent is very low, the LCPC method, which predicts a higher ultimate capacity, should be closer to the pile load test results than the Eslami and Fellenius method. Both

methods exhibit some discrepancies in load-transfer within marl, with higher toe resistance compared to the results from the pile load test.

For T1-18PSC, the LCPC method overestimates the ultimate capacity by approximately 10%. The Eslami and Fellenius method closely aligns with the load-displacement curve. The axial force distributions predicted by both methods are very similar and closely correspond to the measured distribution.

2.6 Discussion and implications

The verification of CPT-based pile resistance estimation and *t-z* and *Q-z* method simulation demonstrate that the numerical model, calibrated using the developed correlations for CPT-based inputs, generally provides a reasonable prediction of pile behavior in marl. However, certain discrepancies exist, particularly in the load-transfer of the T1-P1 pile and the load-displacement of the T1-18PSC. Several potential reasons for these discrepancies will be discussed below, including the variability in marl properties, limitations in CPT data interpretation, and simplifications in the model:

(1) Impact of variability in marl properties: Although marl is relatively more consistent than other soil layers at this site, there is still potential variability, including differences in strength, stiffness, and other geotechnical properties, which can vary significantly over short distances.

(2) Limitations of CPT data interpretation: Cone Penetration Tests (CPT) are used to assess these properties, but their interpretation relies on empirical correlations and assumptions that may not fully capture the inherent variability of marl. Limited CPT points can miss spatial variations and localized anomalies, leading to incomplete or inaccurate

representations of soil behavior. Consequently, the mechanical behavior of marl at specific locations may not be accurately captured, affecting the reliability of predictions for pile performance. These limitations may introduce errors in the back-calculated model inputs. Moreover, the influence zone defined for averaging cone resistance (2*B* above and 4*B* below the pile tip) may not accurately represent the actual stress distribution in all cases.

(3) Simplifications in numerical modeling and limited study cases: The numerical model in this study simplifies complex soil-pile interaction mechanisms, particularly when addressing strain-softening behavior in marl, which can introduce specific errors into the *t-z* method. One such simplification involves the assumption of uniform soil properties along the pile length. This is a significant limitation because soil properties, including strength, stiffness, and density, often vary considerably with depth. These variations, if not accurately represented, can lead to substantial inaccuracies in model predictions. Additionally, the implementation of this *t-z* method assumes elastic behavior for the soil-pile system. This assumption does not account for the plastic behavior of soils, which can result in errors in predicting load-displacement behavior. Moreover, the method typically assumes instantaneous load transfer from the pile to the soil, disregarding time-dependent behaviors such as creep or rate effects. Soils like marl can exhibit significant time-dependent deformations, which are not captured by this simplification. These time-dependent deformations can significantly influence the load-bearing capacity and settlement of piles over time, leading to potential discrepancies between predicted and actual pile performance. Olson (2022) showed that the long-term gain in pile resistance was significant, with capacity increasing by over 500% after a setup period of 17 to 38 days, highlighting the potential for dramatic increases in pile capacity due to time effects.

The outcomes of this study can be developed into a practical tool for routine design. Fig. 2-24 outlines the process for applying this tool, and the recommended model inputs are detailed in Table 2-11.

Table 2-11. Summary of suggested model inputs

Type	LCPC		Eslami and Fellenius		u_{su} (mm)	u_{tu} (mm)	β_s	β_t
	K_s	K_t	C_s	C_t				
PACIP	0.027	0.592	0.035	0.658	8	6	0.9	0.9
DACIP	0.034	0.666	0.045	0.740	17	17	0.92	0.92
Driven	0.044	0.717	0.058	0.925	9	7	0.9	0.9

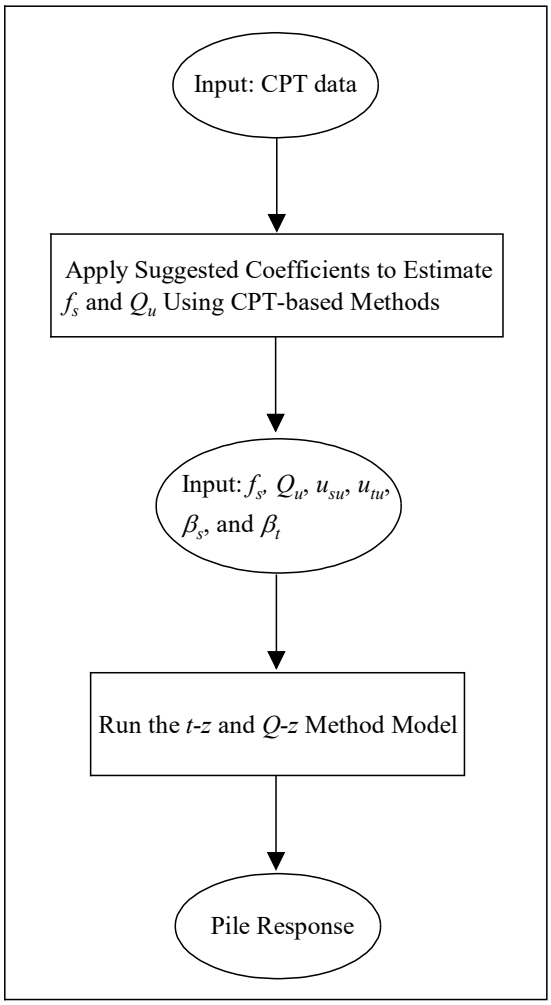

Fig. 2-24. Flowchart for estimating pile resistance and analyzing pile response in marl

2.7 Conclusions

This study outlines a pile load test program and the development of coefficients for CPT-based methods in pile resistance estimation, which are then utilized as inputs for the proposed *t-z* and *Q-z* method model. The study leads to the following conclusions:

- The original LCPC method exhibits significant errors when applied to marl due to its development for bored piles rather than driven piles, disregard for pore pressure on the CPT cone shoulder, use of vertical total stress instead of effective stress, and the imposition of unjustified upper limits on unit shaft resistance.
- The improved correlation coefficients for the LCPC method result in an error range of -13.7% to 7.2%, a significant improvement over the original coefficients, which underestimated pile resistance by up to 86.2%, leading to excessively conservative and costly designs.
- The improved correlation coefficients for the Eslami and Fellenius method result in errors ranging from -35.7% to -5.2%, providing a conservative estimate within an acceptable range. In contrast, the original coefficients led to overestimations of up to 52.1%.
- The calibrated *t-z* and *Q-z* curves developed in MATLAB generally yield accurate predictions of capacity, settlement, and load-transfer. Based on the verification results, using the shaft and toe resistance parameters correlated from both the LCPC and Eslami and Fellenius methods, the ultimate capacity shows an error of less than 10% compared to the pile load test results. Additionally, the load-transfer predictions match the pile load test results fairly well.

References

ASTM International. (2007). “Standard test methods for deep foundations under static axial compressive load (D 1143/D 1143M – 07).” ASTM International, West Conshohocken, PA.

Bustamante, M., and Gianeselli, L. (1982). “Pile bearing capacity prediction by means of static penetrometer CPT.” Proc., Second European Symp. on Penetration Testing, May 24-27, 1982, Amsterdam, Laboratoire Central des Ponts et Chaussées, Paris, France.

Camp, W. M., and Parmar, H. S. (1999). “Characterization of pile capacity with time in the Cooper Marl: Study of applicability of a past approach to predict long-term pile capacity.” Transp. Res. Rec., 1663(1), 16-24.

Crispin, J. J., Vardanega, P. J., and Mylonakis, G. (2019). “Prediction of pile settlement using simplified models.” Proc., XVII ECSMGE-2019: Geotechnical Engineering foundation of the future, Article 0388, Icelandic Geotechnical Society.

Eslami, A., and Fellenius, B. H. (1997). “Pile capacity by direct CPT and CPTu methods applied to 102 case histories.” Can. Geotech. J., 34(6), 886-904.

Fellenius, B. H. (2001). “From strain measurements to load in an instrumented pile.” Geotech. News Mag., 19(1), 35–38.

Fellenius, B. H. (2009). “Views on accuracy of tests and analyses.” Piling & Deep Foundations Asia 2009, Workshop A, July 13, 2009, Sidney, BC, Canada.

Fellenius, B. H. (2013). “Capacity and load-movement of a CFA pile: A prediction event.” ASCE GeoInstitute Geo Congress San Diego, March 3-6, 2013, Foundation Engineering in the Face of Uncertainty, ASCE, Reston, VA, James L. Withiam, Kwok-Kwang Phoon, and Mohamad H. Hussein, eds., Geotechnical Special Publication, GSP 229, pp. 707-719.

Fellenius, B. H. (2017). “Report on the B.E.S.T. prediction survey of the 3rd CBFP event.” Proc., 3rd Bolivian Int. Conf. on Deep Foundations, Santa Cruz de la Sierra, Bolivia, April 27-29, Vol. 3, 7–25.

Fellenius, B. H., and Rahman, M. M. (2019). “Load-movement response by *t-z* and *q-z* functions.” Geotech. Eng. J. of the SEAGS & AGSSEA, 50(3), 11–19.

Kraft, L. M., Ray, R. P., and Kagawa, T. (1981). “Theoretical *t-z* curves.” J. Geotech. Eng. Div., 107(11), 1543–1561.

Lam, C., and Jefferis, S. A. (2011). “Critical assessment of pile modulus determination methods.” Can. Geotech. J., 48(10), 1433–1448.

Lee, K. M., and Xiao, Z. R. (2001). “A simplified nonlinear approach for pile group settlement analysis in multilayered soils.” Can. Geotech. J., 38(5), 1063–1080.

Lin, G. M., and Lin, C. (2019). “Driven pile supported LNG tank in Savannah, Georgia.” Deep Foundation Institute Magazine, Jan/Feb Issue (cover feature) (invited article).

Olson, S. J. (2022). “Driven pile design: An alternative considering pile behavior under service and drag loads.” Geo-Congress 2022, ASCE, Minneapolis, 263-272.

Tan, Y., and Lin, G. (2014). “Comprehensive load test on prestressed concrete piles in alluvial clays and marl in Savannah, Georgia.” J. Perform. Constr. Facil., 28(1), 178-190.

Vardanega, P. J. (2015). “Sensitivity of simplified pile settlement calculations to parameter variation in stiff clay.” In M. G. Winter, D. M. Smith, P. J. L. Eldred, and D. G. Toll, eds., Geotechnical Engineering for Infrastructure and Development: Proc., XVI European Conf. on Soil Mech. and Geotech. Eng., 7, 3777–3782. Thomas Telford, London.

Wang, Z., Xie, X., and Wang, J. (2012). “A new nonlinear method for vertical settlement prediction of a single pile and pile groups in layered soils.” Comput. Geotech., 45, 118–126.

Williamson, M. G. (2014). “Tunnelling effects on bored piles in clay.” Doctoral thesis, University of Cambridge, Cambridge, U.K.

Xiao, H. B., Luo, Q. Z., Tang, J., and Li, Q. S. (2002). “Prediction of load-settlement relationship for large-diameter piles.” Struct. Design Tall Build., 11(4), 285–293.

Yetginer, A. G., White, D. J., and Bolton, M. D. (2006). “Field measurements of the stiffness of jacked piles and pile groups.” Géotechnique, 56(5), 349–354.

Zhang, Q., and Zhang, Z. (2012). “A simplified nonlinear approach for single pile settlement analysis.” Can. Geotech. J., 49(11), 1256–1266.

Zhang, Q., Li, L., and Chen, Y. (2014). “Analysis of compression pile response using a softening model, a hyperbolic model of skin friction, and a bilinear model of end resistance.” J. Eng. Mech., 140(1), 102–111.

Chapter 3

3. Finite Element Analysis of Pile Load Tests on Driven Piles in Marl in Savannah, Georgia

3.1 Introduction

Stiff marl, found in coastal regions such as South Carolina and Savannah, Georgia, is characterized by its calcareous composition, brittleness, and high strength. This soil is highly over-consolidated and typically very uniform, making it a preferred bearing stratum for pile foundations due to its initial strength, consistency, and stability (Camp and Parmar, 1999). These properties make stiff marl an ideal choice for supporting heavy structures, providing a robust foundation capable of withstanding significant loads. However, despite these advantageous properties, engineers face two primary challenges when designing piles in stiff marl. First, the commonly used CPT-based estimations of pile shaft resistance and toe resistance in marl are unreliable. As a result, engineers often rely on pile load test results or empirical values derived from previous pile load tests conducted at other sites. The second challenge is that the over-consolidated marl exhibited the strain-softening response, which can cause pile to plunge when subjected to axial loading. It is generally challenging to numerically simulate the pile plunge response due to the marl's strain-softening behavior, which requires applying an advanced material model as well as large-deformation numerical techniques.

The 3D continuum finite element method (FEM) has been widely used to simulate axially loaded piles; however, a successful simulation of pile plunge that can occur in highly over-consolidated soils has rarely been reported. Over-consolidated soils differ from normally

consolidated soils by exhibiting a lower void ratio, higher strength, and a combination of stress dilatancy with strain softening failure during the post-peak phase (Yao et al., 2008). To better capture these distinctive characteristics of over-consolidated clay (OCC) deposits, several researchers, including Pender (1978), Hueckel et al. (1992), Whittle (1993), Mita et al. (2004), Yao et al. (2009), Gao et al. (2017), and Chen and Yang (2017), have proposed various formulations. Recently, Jockovic and Vukicevic (2017) advanced this understanding by implementing a model that uses a state parameter to characterize the consolidation process of clay, effectively simulating the behavior of OCC. This approach combines the framework of critical state mechanics with a bounding surface methodology, further refining the modeling of these complex soil behaviors.

The primary objective of this paper is to develop and calibrate a 3D continuum finite element model involving OC clay model for stiff marl on the basis of the test data. The calibrated numerical model was further applied to simulate an independent pile load test at the same site. While this study is limited to evaluation of the constitutive models, the outcomes would advance the capability of the numerical simulation of pile plunge and provide a valuable reference for the integration of single pile simulation to a large-scale simulation of pile groups containing over thousands of piles. Additionally, this research conducts a parametric study on marl's critical state friction angle and pile dimensions, exploring how variations in the critical state friction angle influence pile response to assess the sensitivity of soil strength parameters and identifying the most influential factors in pile dimensions.

3.2 Subsurface conditions and pile load test program

The subsurface conditions and the pile load test program are detailed in Chapter 2. This study involves test piles, specifically the driven concrete pile T1-18PSC in test area 1 and T2-14PSC in test area 2.

3.3 Finite element modeling

3.3.1 FEM model setup

A 3D continuum FEM model was developed using Plaxis 3D to simulate the pile load tests at Test Area 1 for the T1-18PSC pile, as illustrated in Figs. 3-1 and 3-2. The setup includes material properties, structural details, meshing, boundary conditions, and applied loads.

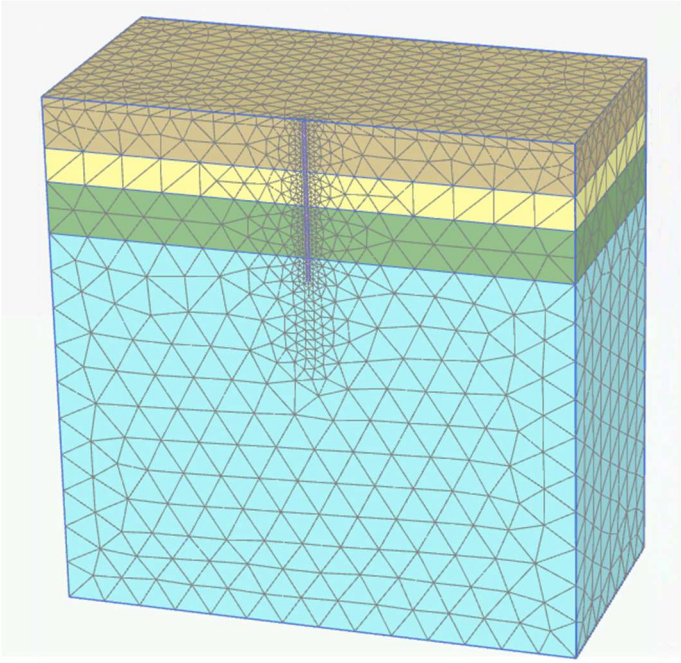

Fig. 3-1. Numerical model geometry

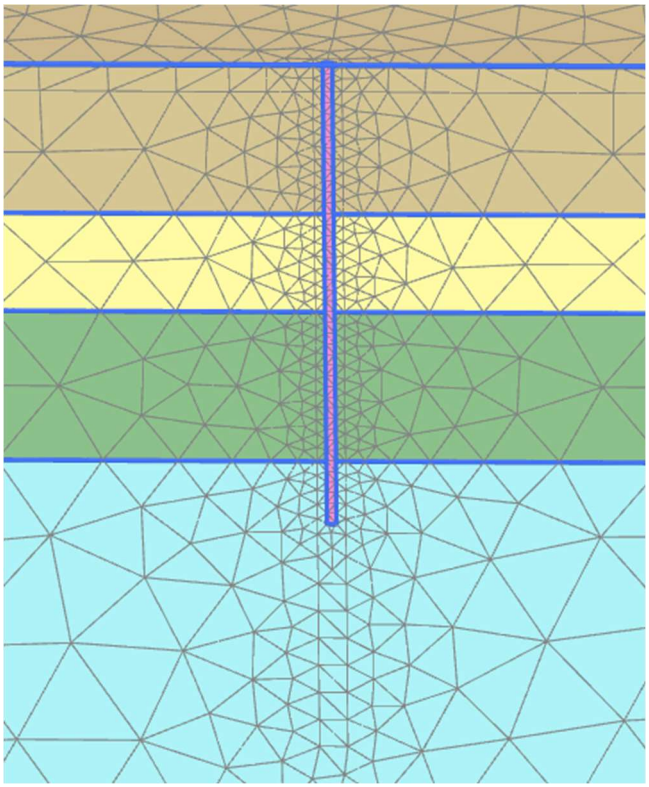

Fig. 3-2. Detailed view of the numerical model mesh

The soil profile consists of multiple layers with varying properties. The first layer, from 0 to 7.8 meters, combines Limestone Aggregates and Very Soft to Soft Organic Clay and is modeled using the Modified Cam-clay model under undrained condition. The second layer, from 7.8 to 13 meters, consists of Soft Clay and Sand Mixture and is modeled by the Mohr-Coulomb model in undrained condition. The third layer, from 13 to 21 meters, is Medium to Dense Sand, modeled by the Hardening Soil model in drained condition. The fourth layer, below 21 meters, is Marl, modeled using the OC Clay model in drain condition as the stiff marl contains sand, allowing pore pressure to dissipate similarly to sand. The pile itself is modeled as purely elastic. Soil model parameters for the OC Clay model were derived from sources including correlation with CPT and shear wave

velocity data, and manual suggestions and experience-based estimations, which are listed in corresponding tables in later section.

The T1-18PSC pile has a side length of 0.46 meters and an embedded length of 24.4 meters. The model uses symmetry as depicted in the provided images.

The model is meshed using 10-noded tetrahedral elements. The meshing process was optimized for both accuracy and efficiency. Around the pile, the mesh was refined with a coarseness factor of 0.25, whereas the rest of the model employed a coarseness factor of 1.0. The refined area dimensions are 1.38 meters in width (three times the pile side length B) and 36.6 meters in depth (1.5 times the pile length L_p).

For a single pile, Murphy et al. (2018) recommends setting the horizontal boundary at forty times the pile diameter or width, and the depth at twice the pile length. In this study, the boundaries were set larger than the suggested values, with dimensions of 80 meters in length, width, and depth, to eliminate any potential boundary effects. Boundary conditions were set to simulate realistic constraints. The bottom boundary was restrained in the vertical direction but free for translational movement. On the top boundary, the soil was not allowed to move horizontally but was free to move vertically. The left and right boundaries were fixed in the horizontal direction but free in the vertical direction.

The loading scheme in the numerical model followed the static loading test program discussed previously.

3.3.2 OC Clay model

The OC Clay model is built upon the Hardening State Parameter (HASP) model, which is specifically designed to enhance the prediction of the stress-strain behavior of over-consolidated clays (OCC). This model offers significant advantages in geotechnical analysis, particularly by

improving the accuracy of modeling post-peak softening behavior in soils. By incorporating the HASP model's framework, the OC Clay model addresses the challenges associated with predicting the complex responses of over-consolidated clays under various loading conditions, ensuring more reliable and accurate simulations of soil-structure interactions.

Fig. 3-3 presents the theoretical framework applied in the OC Clay model. In the upper graph, the vertical axis represents deviatoric stress, while the horizontal axis denotes mean effective stress. This graph illustrates the progression of stress conditions toward the Critical State Line (CSL), where the soil undergoes continuous deformation without further volume change. The Bounding Surface indicates the threshold beyond which the soil experiences significant, irreversible deformations, commonly referred to as 'failure'. In the lower graph, the Normal Consolidation Line (NCL) demonstrates the changes in soil volume under various stress paths, effectively capturing both normal consolidation behavior and the responses during unloading and reloading processes. Importantly, the parameter $\Psi^{\star}$ represents dilation, which is key to the model's ability to simulate 'softening behavior'.

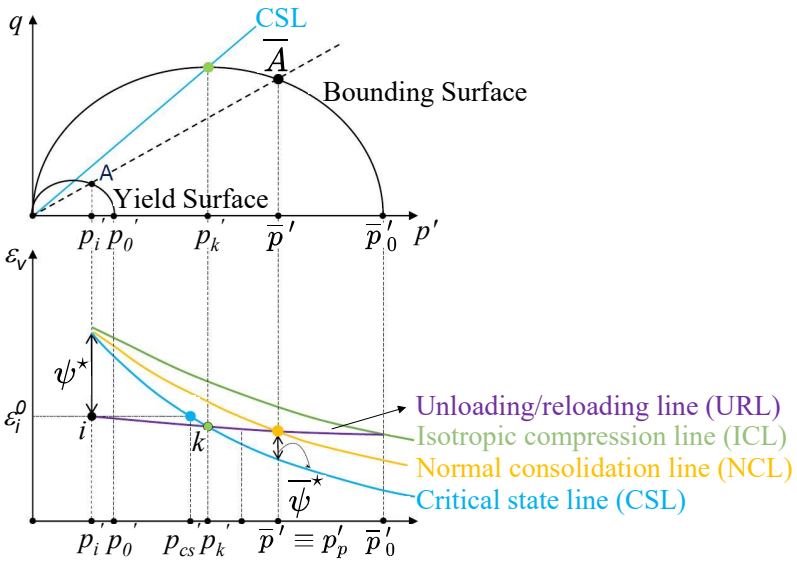

Fig. 3-3. Diagram of the theoretical framework applied in the OC Clay model (Jockovic and Vukicevic, 2017)

The OC Clay model's stiffness parameters are defined by the unloading-reloading Young's modulus (E_{ur}), which is usually obtained from the unloading branch in a triaxial test with intermediate unloading stages and can be calculated using specific equations, the oedometer modulus (E_{oed}) derived from the primary loading branch in a one-dimensional compression test beyond the pre-consolidation stress, and the shear modulus at very small strains (G_0).

The advanced parameters of the OC Clay model include the Poisson's ratio in unloading and reloading (v_{ur}), which describes the soil's elastic behavior, and the reference mean effective stress (p_{ref}), used in stress-dependent stiffness calculations. The friction angle at the critical state (φ'_{cs}) represents the soil's shear strength at large strains, and the earth pressure coefficient at rest (K_0) is used to determine the pre-consolidation state of the soil. Pre-Overburden Pressure (POP) is another essential parameter for calculating the pre-consolidation state of the soil and is defined as:

$$POP = \sigma'_v, max - \sigma'_v \tag{3-1}$$

Where σ_v', max = maximum value due to pre overburden pressure; σ_v' = vertical effective stress in the soil. Additionally, the model includes parameters to adjust the plastic deformability of the soil (h) and a flag to switch from an elasto-plastic response during reloading paths to an elastic behavior (el_{Reload}).

3.3.3 Determination of OC Clay model input parameters

Parameters of OC Clay model are primarily determined from sources including: CPT and shear-wave velocity correlation, and manual suggestions and experience-based estimations as detailed in Tables 3-1 and 3-2. Parameters correlated from CPT and shear-wave velocity are listed below:

Referring to Robertson and Cabal (2014), the soil unit weights (γ) are obtained using CPT data:

$$\frac{\gamma}{\gamma_w} = 0.27\left[logR_f\right] + 0.36[log(q_T/P_a)] + 1.236 \tag{3-2}$$

Where R_f = friction ratio; γ_w = unit weight of water in same unit as γ; q_T = cone resistance adjusted for pore water pressure on shoulder; P_a = atmospheric pressure in same units as q_T.

The small strain shear modulus (G_0) is calculated using:

$$G_0 = \rho V_s^2 \tag{3-3}$$

Where ρ = density of soil; V_s = shear wave velocity.

According to Robertson (2009), the oedometer modulus (E_{oed}) is calculated using the correlation:

$$E_{oed} = \alpha_M (q_T - \sigma_v) \tag{3-4}$$

Where α_M = the constrained modulus cone factor taken as 14 for marl in this study; σ_v = the vertical stress in the soil. The unloading-reloading Young's modulus (E_{ur}) is suggested by the Plaxis 3D material models manual (2024) to be taken as 3 times the E_{oed}.

Table 3-1. Model inputs from CPT and shear-wave velocity correlation

Soil	Model and Drainage Condition	Model Inputs			
Marl	OC Clay	γ (kN/m3)	E_{oed} (MPa)	E_{ur} (MPa)	G_0 (MPa)
	Drained	19.4	99.4	298.2	60

Note: γ = unit weight of soil; E_{oed} = oedometer modulus; E_{ur} = unloading-reloading Young's modulus; G_0 = small strain shear modulus.

As detailed in Table 3-2, for marl, the reference mean effective stress (p^{ref}) is 100 kPa. The threshold shear strain ($\gamma^{0.7}$) and the flag to switch from an elasto-plastic response during reloading paths (el_{reload}) are set to zero, referring to the Plaxis OC Clay Manual (Bentley Systems, Inc., 2023). The parameter used to increase/decrease the plastic deformability of the soil (h) is initially set to 0.5, referencing cases in the Plaxis OC Clay Manual (Bentley Systems, Inc., 2023). The earth pressure coefficient at rest is calculated by K_0 = 1 - sin φ' as suggested by the Plaxis 3D material models manual (2024). Unfortunately, no lab test data is available for the stiff marl at this site

because it is too difficult to sample using a Shelby tube. Mayne and Woeller (2013) presented test data for Cooper marl from a site approximately 100 km from the test area in this study, where the effective friction angle (φ') was estimated to be 41º. Consequently, the critical state friction angle (φ'_{cs}) was initially estimated to be 34º, applying a reduction based on the reported effective friction angle; and the pre-overburden pressure (*POP*) is calculated based on an initial over-consolidation ratio (*OCR*) of 10.

The pile modulus is interpreted from pile load test data using the Tangent Modulus method as detailed in Chapter 2.

Table 3-2. Model inputs from manual suggestions and experience-based estimations

Soil	Model and Drainage Condition	Model Inputs				
Marl	OC Clay Drained	v_{ur}	p^{ref} (kPa)	$\gamma^{0.7}$	φ'_{cs} (º)	K_0
		0.2	100	0	34	0.34
		POP (kPa)	*h*	el_{Reload}		
		1890	0.5	0		
Pile	Linear elastic	γ (kN/m^3)	*E'* (GPa)	*v*		
		24.0	37.9	0.2		

Note: v_{ur} = Poisson's ratio in unloading and reloading; p^{ref} = reference mean effective stress; $\gamma^{0.7}$ = the threshold shear strain at which the secant shear modulus $G_s = 0.722G_0$; φ'_{cs} = critical state friction angle; K_0 = earth pressure coefficient at rest; *POP* = Pre-Overburden Pressure; *h* = Parameter introduced to increase/decrease the plastic deformability of the soil; el_{Reload} = flag to switch from an elasto-plastic response during reloading paths; γ = unit weight of the pile; *E'* = Young's modulus; *v* = Poisson's ratio.

3.3.4 Results and discussion

Fig. 3-4 illustrates the relationship between the applied load and pile head displacement. In the initial elastic behavior, both the simulation (red line) and the pile load test (black line) start similarly, indicating that the initial elastic response of the pile-soil system is well captured by the simulation. However, as the load increases, the simulation begins to diverge from the test results in the post-yield behavior. At a load of around 2000 kN, the simulation shows a sharper increase in displacement compared to the pile load test result.

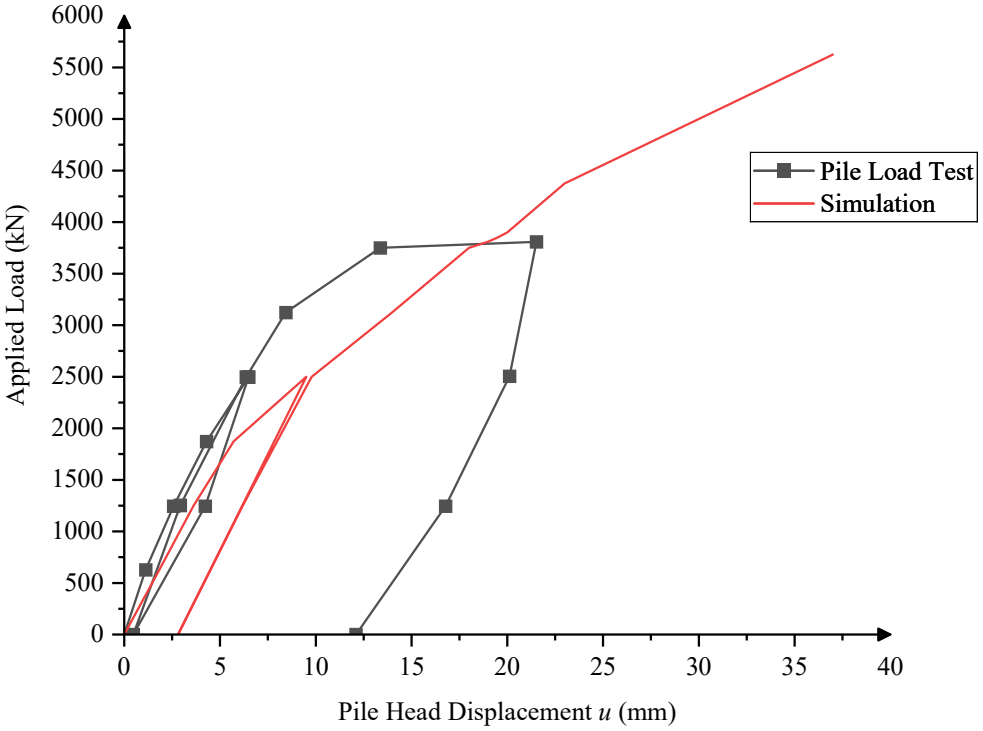

Fig. 3-4. Comparison of load-displacement curves between simulations using correlated inputs and measured data

The peak load and failure are particularly significant. The test results indicate an ultimate capacity of approximately 3810 kN accompanied by substantial displacement, followed by a slight reduction in load-bearing capacity, which signifies plunging failure. In contrast, the simulation does not exhibit this peak as clearly and shows a more steady increase in load. It is important to note that the current FEM in Plaxis 3D was unable to replicate a plunging failure with large displacement at a constant load because such a scenario would distort the mesh, leading to a 'soil body collapse' error in the system.

Furthermore, the displacement at failure in the pile load test shows a higher displacement compared to the simulation. This suggests that the simulation with correlated inputs may overestimate the pile's capacity to undergo large deformations before failure. Improving the soil model to better reflect strain-softening could help address this.

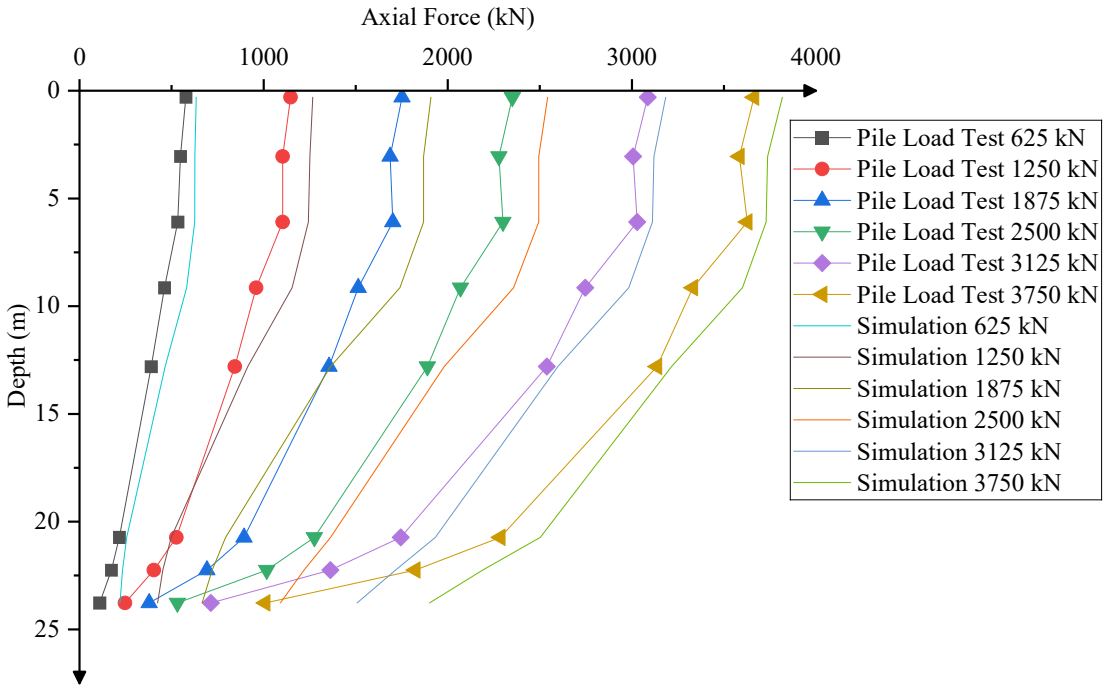

Fig. 3-5. Axial force distribution comparison between simulations using correlated inputs and measured data at various load levels

Fig. 3-5 presents the axial force distribution along the pile depth for various applied loads, providing further insights.

At lower load levels (625 kN - 1250 kN), the simulation results align closely with the test data, indicating accurate modeling of the pile-soil interaction in the initial loading stages. The force distribution is smooth and shows a gradual reduction with depth, consistent with the test results.

As the applied load increases to intermediate levels (1875 kN - 3750 kN), certain discrepancies become evident. The simulation generally shifts the axial force from the top of the pile towards the bottom. There is a significant discrepancy in shaft and toe resistance in marl. At the highest load level (3750 kN), the differences are more pronounced. The test results show a sharper drop in axial force in marl compared to the simulation. The simulation indicates a more gradual load transfer. This reinforces that the soil model parameters derived from correlations might not fully

capture the complex behavior of marl, and the need for a more detailed calibration of the soil models.

3.4 Model calibration and validation

3.4.1 Calibrated model inputs

The calibration was performed on the OC Clay layer for marl, while the remaining soil layers were set to align with the load-transfer observed in the pile load test. Primary parameters such as the oedometer modulus (E_{oed}) for stiffness and the critical state friction angle (φ'_{cs}) for strength are adjusted, with E_{oed} being fine-tuned within a narrow range and φ'_{cs} receiving particular attention due to the model's sensitivity to this parameter, while the remaining model inputs are kept consistent. The fitting process is illustrated in Figs. 3-6 and 3-7, and Table 3-3 provides details on the model inputs adjusted for better alignment between the simulation and pile load test results.

For the load-displacement response, one of the critical aspects was capturing the peak load accurately. The calibrated curve provided a more precise representation of the peak load. Although the curve did not fully replicate the whole process of plunging failure observed in the tests, the adjustments made during the calibration process brought the model closer to these conditions.

Regarding the axial force distribution, in the marl layer (from a depth of 21 m), an excessively large portion of the resistance was attributed to the shaft (as indicated by the slope of the axial force distribution curve). Due to software limitations, achieving perfect alignment through input adjustments alone was not possible.

Table 3-3. Model inputs adjusted during calibration

Soil	Model and Drainage Condition	Model Inputs			
Marl	OC Clay Drained	E_{oed} (MPa)	E_{ur} (MPa)	φ'_{cs} (°)	K_0
		88	264	27	0.43

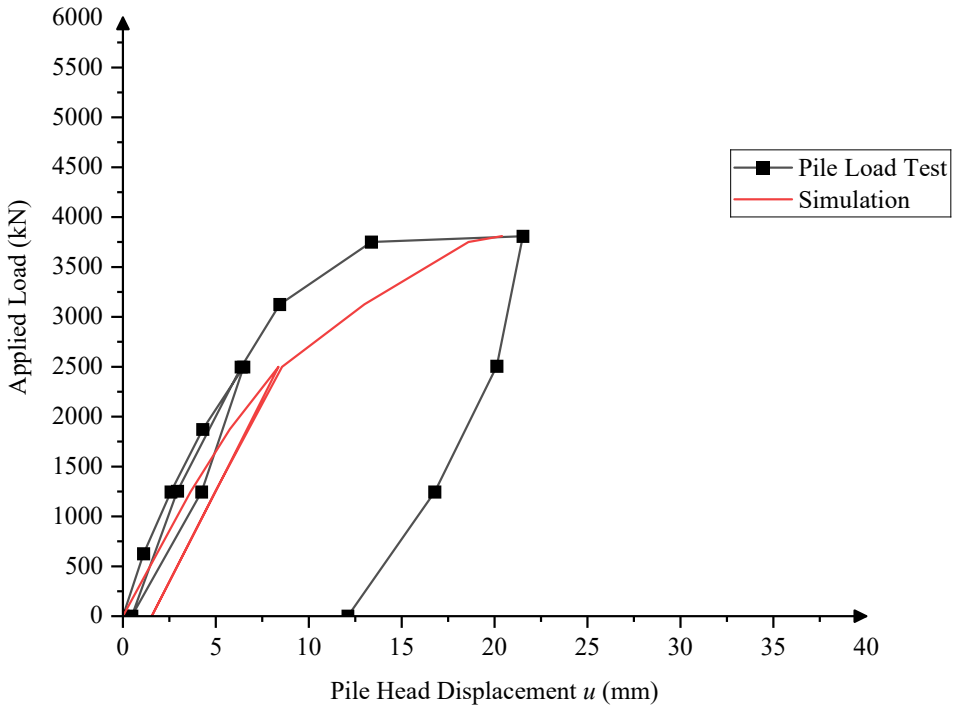

Fig. 3-6. Comparison of load-displacement curves between simulations after calibration and measured data

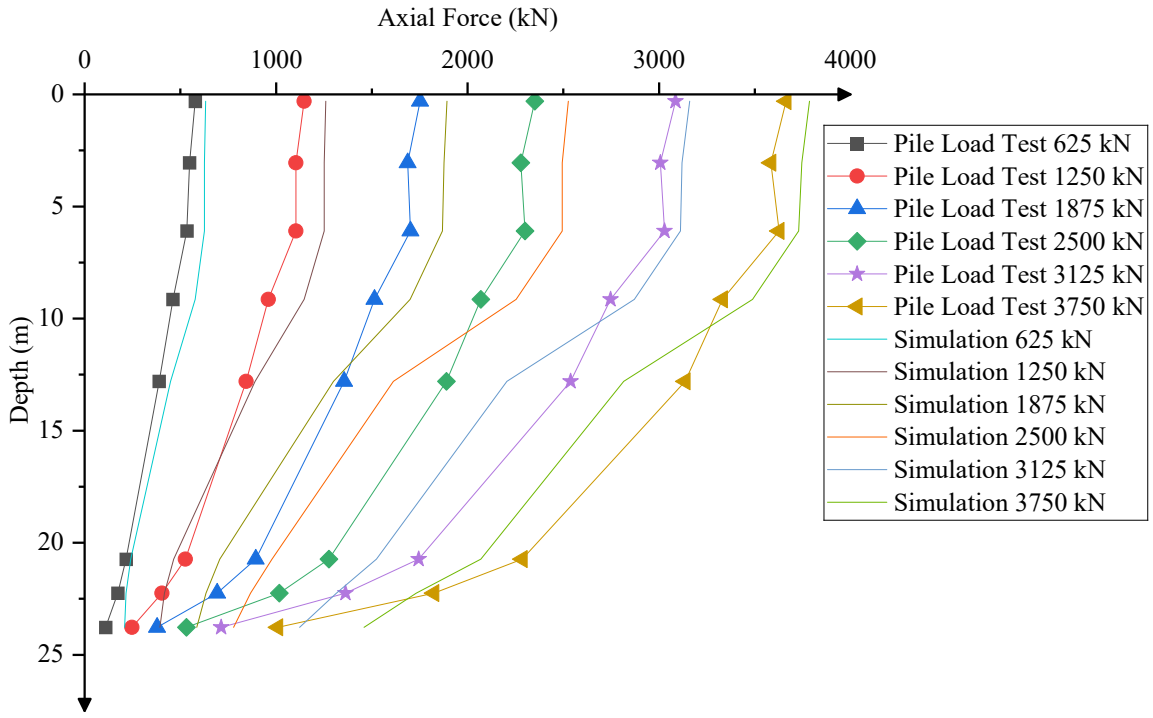

Fig. 3-7. Axial force distribution comparison between simulations after calibration and measured data at various load levels

3.4.2 Verification of the FEM model

The model is verified using the pile load test of T2-14PSC in Test Area 2.

As detailed in Table 3-4, the oedometer modulus (E_{oed}) is calculated using the same correlation as mentioned previously but is multiplied by a reduction factor of 88.5%, reflecting the reduction of this parameter after calibration. Model inputs including the soil unit weight (γ), the small strain shear modulus (G_0), and the unloading-reloading Young's modulus (E_{ur}) remain the same correlated value, while other inputs remain consistent with the calibrated model from the previous section. The modulus of pile T2-14PSC is interpreted from pile load test data using the Tangent Modulus method as detailed in Chapter 2.

Table 3-4. Model inputs for verification of the FEM model

Soil	Model and Drainage Condition	Model Inputs				
Marl	OC Clay Drained	γ (kN/m^3)	E_{oed} (MPa)	E_{ur} (MPa)	G_0 (MPa)	K_0
		19.7	66	198	80	0.43
		ν_{ur}	p^{ref} (kPa)	$\gamma^{0.7}$	φ'_{cs} (°)	POP (kPa)
		0.2	100	0	27	1500
		h	el_{Reload}			
		0.5	0			
Pile	Linear elastic	γ (kN/m^3)	E' (GPa)	ν		
		24.0	36.8	0.2		

Note: γ = unit weight of soil; E_{oed} = oedometer modulus; E_{ur} = unloading-reloading Young's modulus; G_0 = small strain shear modulus; K_0 = earth pressure coefficient at rest; ν_{ur} = Poisson's ratio in unloading and reloading; p^{ref} = reference mean effective stress; $\gamma^{0.7}$ = the threshold shear strain at which the secant shear modulus G_s =0.722G_0; φ'_{cs} = critical state friction angle; POP = Pre-Overburden Pressure; h = Parameter introduced to increase/decrease the plastic deformability of the soil; el_{Reload} = flag to switch from an elasto-plastic response during reloading paths; γ = unit weight of the pile; E' = Young's modulus; ν = Poisson's ratio.

Figs. 3-8 and 3-9 provide insights into the model's accuracy.

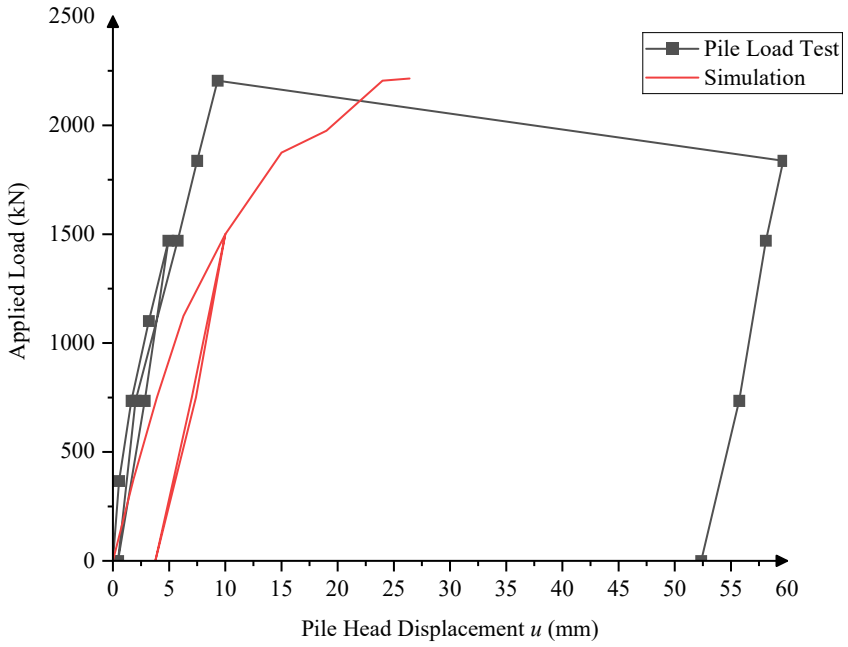

Fig. 3-8. Comparison of load-displacement curves between verification and measured data

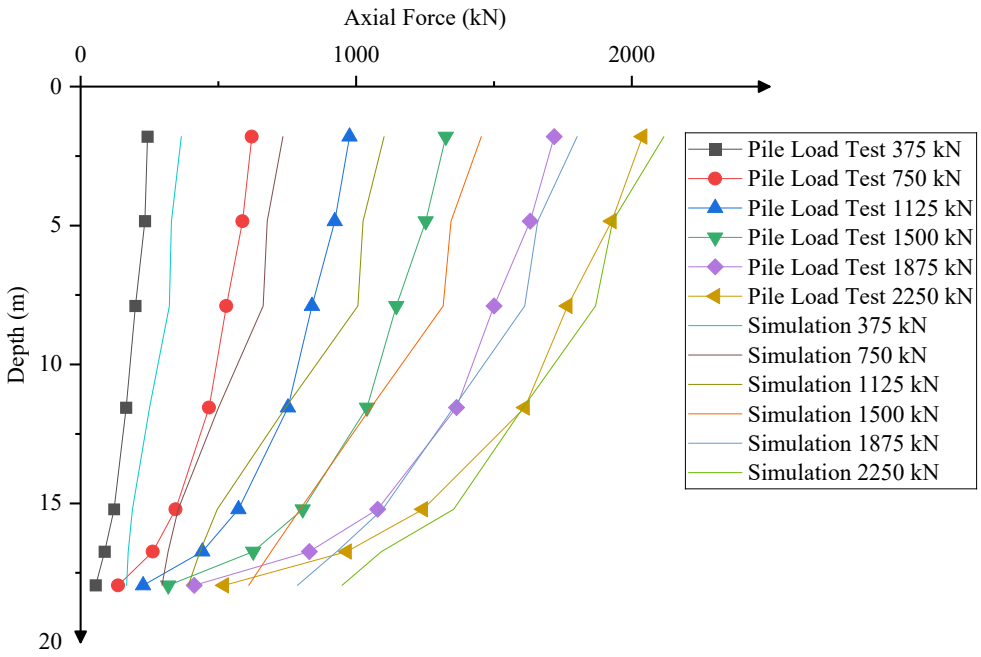

Fig. 3-9. Axial force distribution comparison between verification and measured data at various load levels

The load-displacement curve indicates that both the simulation and the pile load test exhibit similar elastic behavior during the initial loading stages, suggesting that the model parameters for the elastic range are reasonably accurate. As the load increases, some discrepancies occur. In terms of peak load and failure, the test results indicate a peak load of approximately 2205 kN with substantial displacement, followed by a reduction in load-bearing capacity, signifying soil failure or significant yielding. While the simulation does not perfectly replicate the plunging failure observed in the tests, it now approximates these conditions more closely after calibration.

The axial force distribution along the pile depth for various applied loads indicates that the general trend of load transfer from the pile to the surrounding soil is well represented. The load transfer within the marl layer (from a depth of 15.5 m), the distribution of shaft and toe resistance follows the established pattern but exhibits some discrepancies when compared to the pile load test results. Similar to T1-18PSC in test area 1, an excessively large portion of the resistance was

attributed to the shaft, as indicated by the slope of the axial force distribution curve. Due to software limitations, achieving perfect alignment through input adjustments alone was not feasible.

3.5 Parametric study

To compare the simulation outcomes in the subsequent parametric study, it is essential to quantify the capacity derived from the simulations. Various criteria, such as 5% of the pile side length criteria proposed by FHWA (2007), have been proposed to interpret the ultimate bearing capacities of the piles under axial compression loads. Moreover, by analyzing the load-settlement curve obtained from the pile loading tests, many graphical methods developed by Davisson (1972), Decourt (1999), Corps of Engineers (1991), and Fuller and Hoy (1970) have been proposed to find the pile bearing capacity (Olgun et al., 2017). Since the ratio of settlement/B observed in the simulation results is relatively small, methods like the 5%B criterion (where B is the pile side length) are not suitable. Therefore, Davisson method proposed by Davisson (1972), Corps of Engineers Method and Tangent method were used to interpret the ultimate compression capacity (or the maximum compressive loads) from the simulations. Davisson's method involves two steps. First, plot a linear pile deformation line and offset it from the origin by (0.15 + B/120) inches (B is the pile side length). Second, the maximum compressive load is taken at a point corresponding to the interception between the offset linear line and the measured load-settlement curve. In Tangent Method, the ultimate bearing capacity of piles is determined by first drawing tangent lines to the initial and final portions of the load-settlement curves. The intersection point of these two tangents is considered to represent the ultimate bearing capacity of the pile. The Corps of Engineers Method is primarily used by the U.S. Army Corps of Engineers (1991). In this method, the load-settlement curve is drawn first, and then three different loads are detected. The first load (Q_1) is

the load corresponding to the 6.4 mm settlement level. The second load (Q_2) is the load corresponding to the point obtained by the tangential method. The third load (Q_3) is the load corresponding to the point where the line makes an angle of 0.025 mm/kN intersects with the load-settlement curve. The average of these three load values is considered the ultimate bearing capacity of the pile.

3.5.1 Critical state friction angle

Using the previously calibrated and validated models, a numerical parametric study was conducted to better understand the performance of single piles under varying conditions. This section focuses on the impact of changing the critical state friction angle (φ'_{cs}) while keeping other parameters constant.

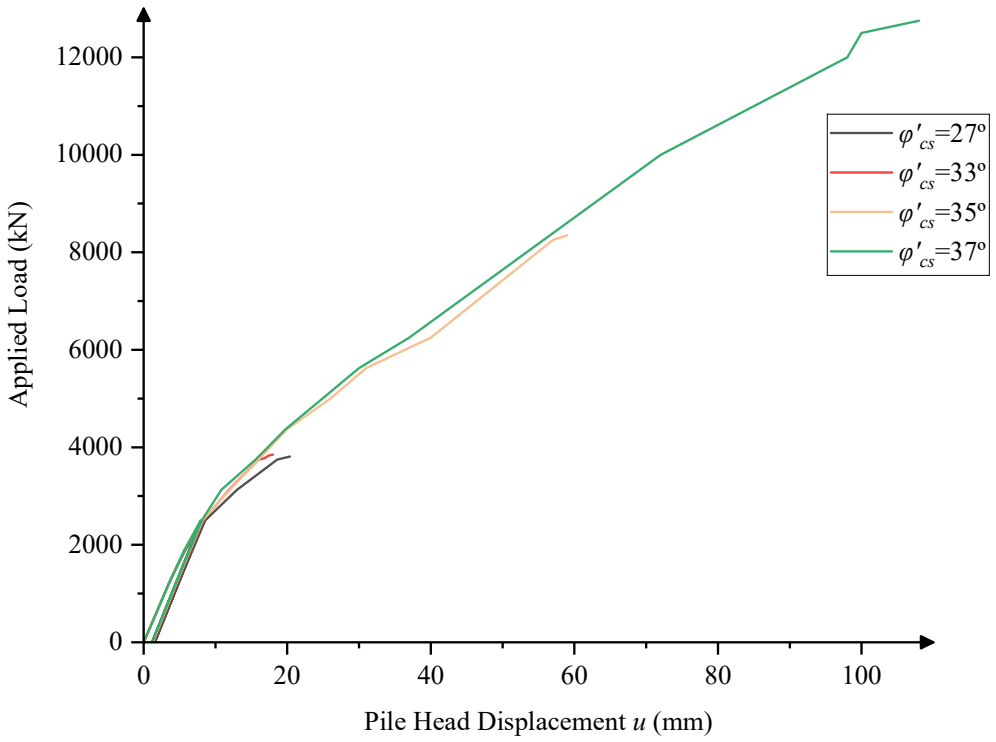

Fig. 3-10. Load-displacement curves for different critical state friction angles (φ'_{cs})

The load-displacement curve in Fig. 3-10 reveals that when the critical state friction angle varies from 27° to 33°, the settlement response remains relatively unchanged, with smaller displacement at the same load when φ'_{cs} =33° compared to φ'_{cs} =27°. This indicates that within this range, the soil-pile interaction is not significantly sensitive to changes in φ'_{cs}. However, as the critical state friction angle increases further to 35° and 37°, a noticeable increase in bearing capacity is observed. This suggests that at higher values, even small increments in φ'_{cs} can substantially enhance the pile's load-bearing performance.

Table 3-5 summarizes the ultimate bearing capacities determined using the Corps of Engineers Method, Tangent Method, and Davisson method for different values of φ'_{cs}. It is evident that as φ'_{cs} increases, all methods show a rise in the calculated bearing capacities.

Table 3-5. Summary of interpreted capacities for different values of φ'_{cs}

Capacity (kN) \ φ'_{cs} (°)	27	33	35	37
Corps of Engineers Method	3092	3169	5767	8383
Tangent Method	3500	3625	6900	10400
Davisson Method	3760	3800	4000	4100

The axial force distribution along the pile depth for various applied loads, as illustrated in Fig. 3-11, reveals a general trend: within the concerned load range, higher critical state friction angles result in a greater portion of the bearing capacity being contributed by the pile toe compared to lower critical state friction angles.

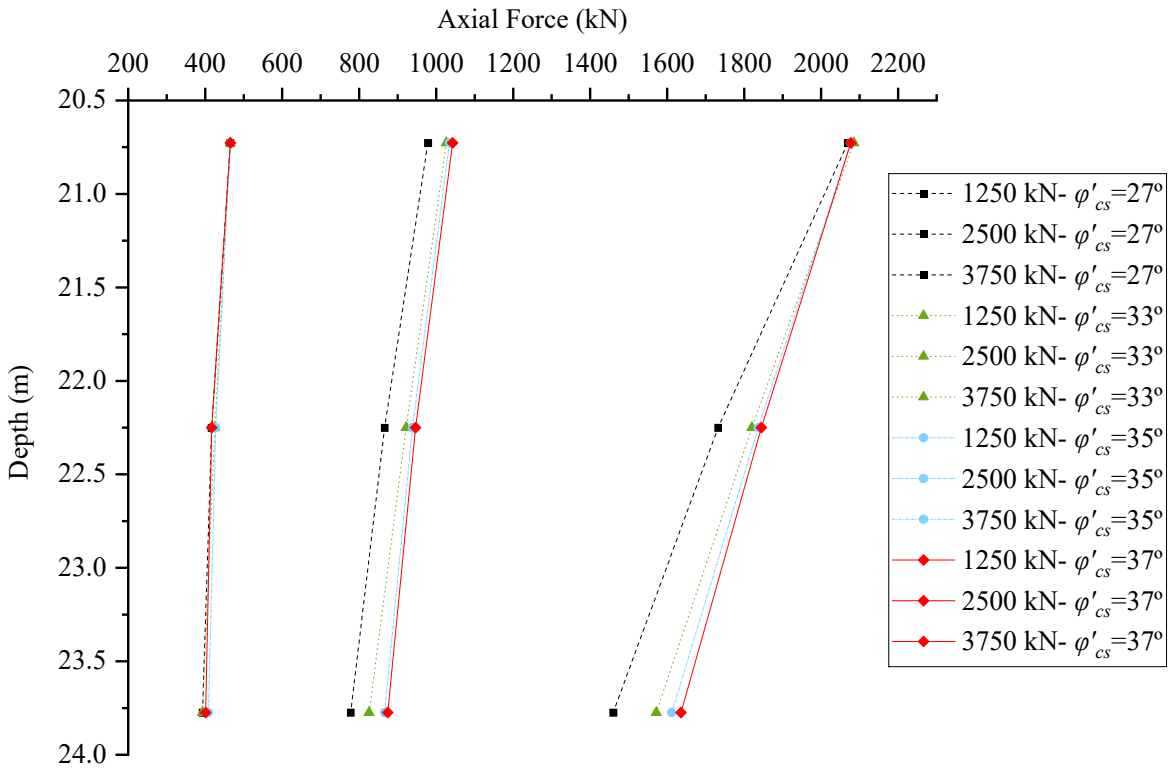

Fig. 3-11. Axial force distribution along the pile depth for various applied loads and critical state friction angles (φ'_{cs})

In conclusion, the parametric study underscores that while minor changes in φ'_{cs} within a low range have limited impact on settlement and bearing capacity, higher values of φ'_{cs} result in significant sensitivity to changes and substantial improvements with small adjustments. This highlights the importance of precise soil characterization in geotechnical designs to optimize pile performance effectively.

3.5.2 Pile side length

This section focuses on the impact of changing the pile side length from 0.36 m (i.e., 14 inches) to 0.46 m (i.e., 18 inches), and finally to 0.56 m (i.e., 22 inches) while keeping other parameters constant.

The load-displacement curve in Fig. 3-12 reveals a significant impact of pile side length on settlement response. As the side length increases, the pile exhibits a higher bearing capacity and reduced displacement for the same load. Specifically, larger side lengths show substantially greater load-bearing capacities. The normalized load-displacement curve in Fig. 3-13 further illustrates this trend. The curves indicate that as the side length increases, the load capacity at a given normalized displacement (u/B) also increases. This suggests that larger side length piles not only have a higher absolute bearing capacity but also perform better relative to their size, demonstrating greater efficiency in load-bearing capacity.

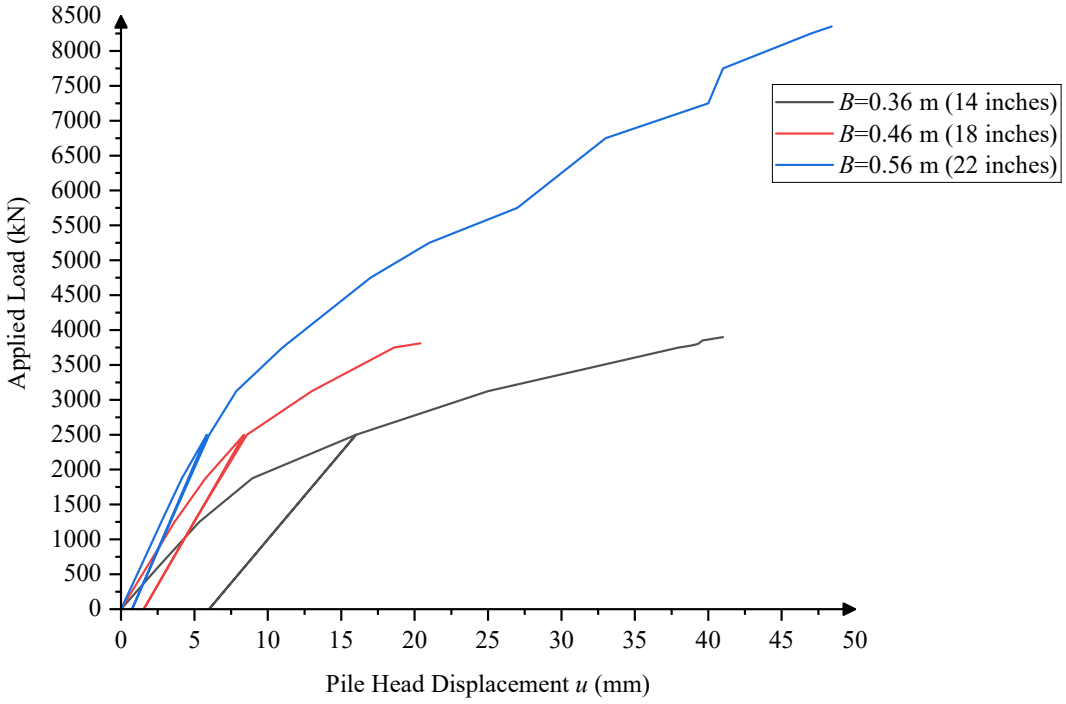

Fig. 3-12. Load-displacement curves for different pile side length *B*

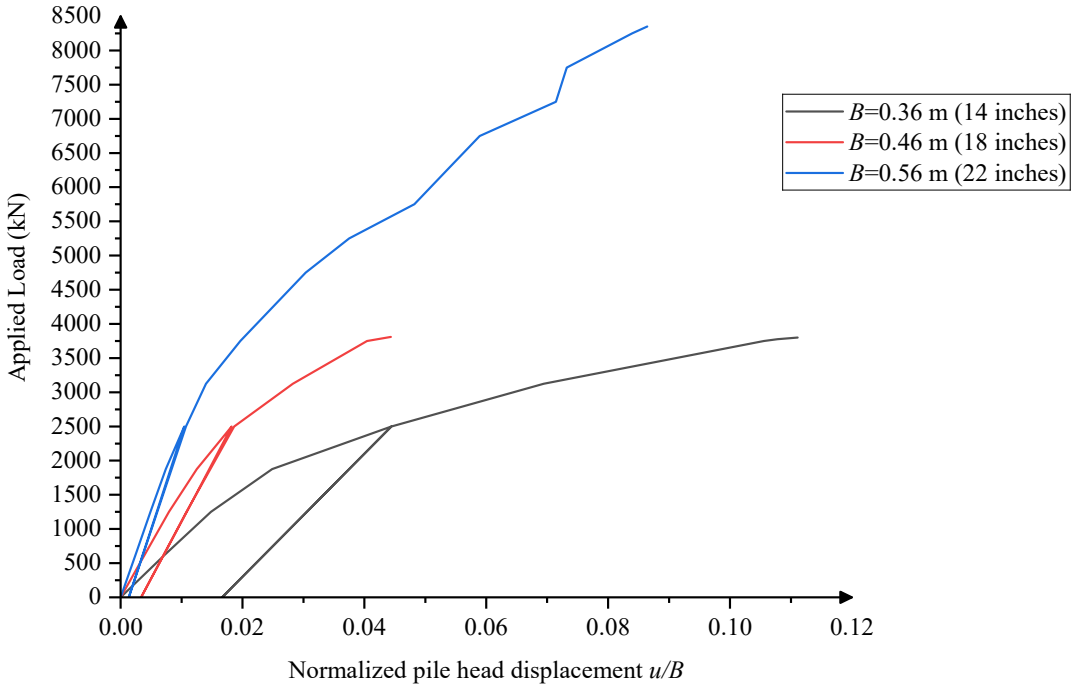

Fig. 3-13. Normalized load-displacement curves for different pile side length *B*

Table 3-6 summarizes the ultimate bearing capacities determined by different methods for different pile side length. From the table, reasonably, as the pile side length increases, the capacity shows a significant rise.

Table 3-6. Summary of interpreted capacities for different pile side length *B*

B (m) / Capacity (kN)	0.36	0.46	0.56
Corps of Engineers Method	2781	3169	5275
Tangent Method	3125	3625	5450
Davisson Method	2450	3800	5050

The axial force distribution along the pile depth for various applied loads in Fig. 3-14 indicates that larger side length piles distribute more load through shaft friction compared to smaller side length piles (except at very low load level). As the pile side length increases, a greater proportion

of the load is carried by shaft friction rather than end-bearing. This distribution of axial forces underscores the efficiency of larger side length piles in utilizing shaft resistance to support loads. It should be noted that the comparison is limited to head loads ranging from 1250 kN to 3750 kN, where toe resistance should not have been fully mobilized for the pile with B = 0.56 m. Under higher loading conditions, it is reasonable to expect that toe resistance will take on a larger portion of the load, as shaft resistance would be fully mobilized at an earlier stage.

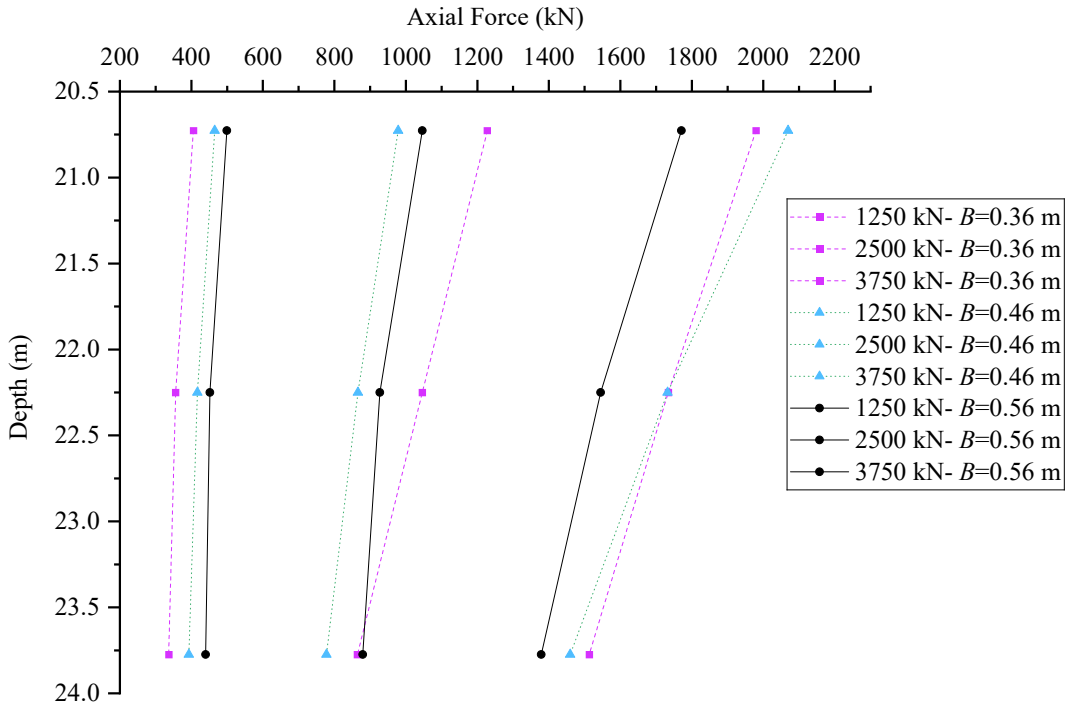

Fig. 3-14. Axial force distribution along the pile depth for various side length *B*

In conclusion, the parametric study highlights the substantial impact of pile side length on settlement response and bearing capacity. Larger side lengths lead to significant improvements in load-bearing performance, primarily due to increased shaft friction.

3.5.3 Embedment length

When designing pile foundations in this area, it is recommended to specify a predetermined depth of penetration into the marl rather than a pile tip elevation. This approach ensures that the surface area is adequate to develop sufficient shaft resistance to support the design load (Baus and Ray 1988). This section will examine the impact of varying embedment lengths into marl on the pile response.

The load-displacement curve in Fig. 3-15 shows that piles with greater embedment lengths reasonably have higher load-bearing capacities. Specifically, a pile with an embedment length of 5.1 m supports the highest load with less displacement compared to piles with shorter embedment lengths. This indicates that deeper embedment enhances the pile's load-bearing performance and reduces settlement under the same applied loads.

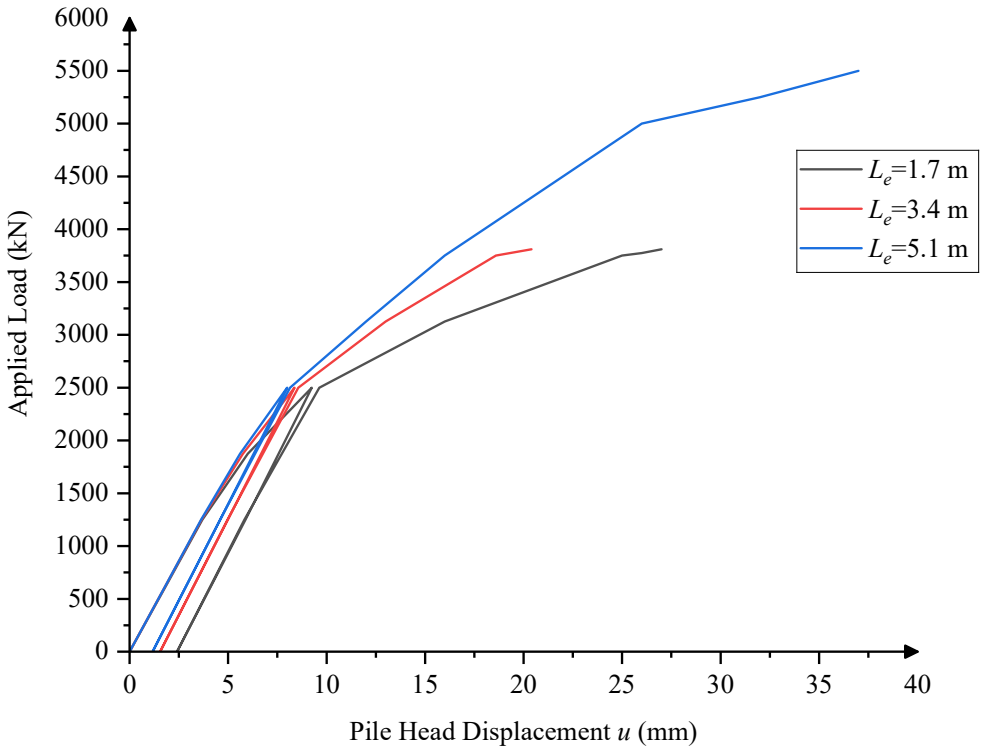

Fig. 3-15. Load-displacement curves for different embedment length into marl

Table 3-7 summarizes the ultimate bearing capacities determined using different methods. It shows a significant increase in bearing capacity with increasing embedment length, particularly for the longest embedment length of 5.1 m.

Table 3-7. Summary of interpreted capacities for different embedment lengths

Capacity (kN) \ Embedment Length (m)	1.7	3.4	5.1
Corps of Engineers Method	2819	3169	3800
Tangent Method	3375	3625	4400
Davisson Method	3167	3800	4583

The axial force distribution along the pile depth for various applied loads in Fig. 3-16 indicates that while longer embedment lengths generate more shaft resistance due to increased surface area, the slope of the axial force is steeper compared to shorter embedment lengths, suggesting less unit shaft resistance.

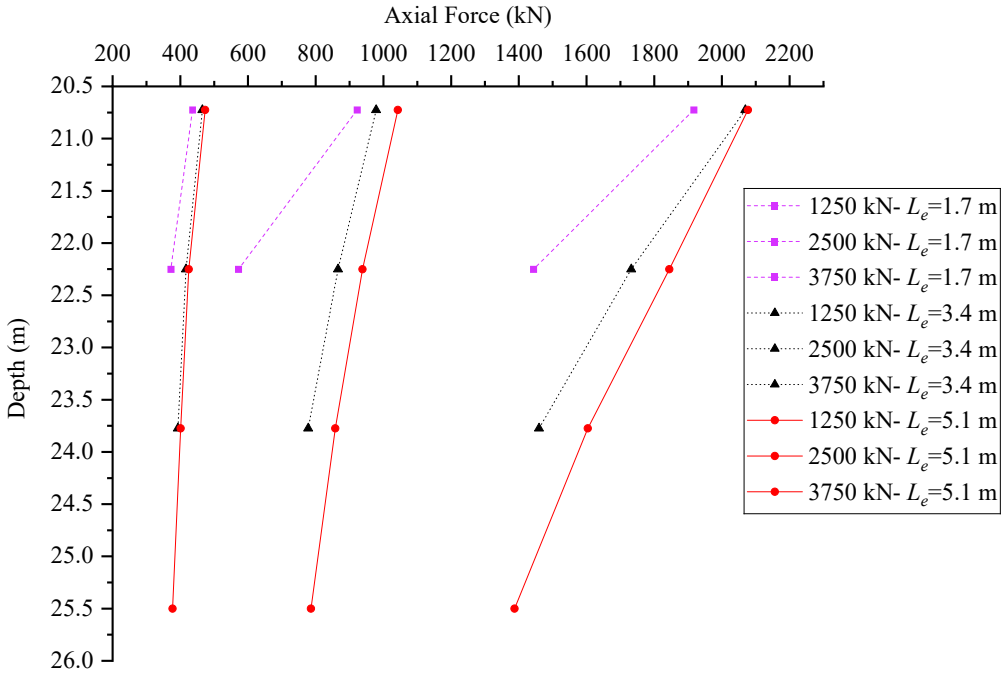

Fig. 3-16. Axial force distribution along the pile depth for various embedment length into marl

3.6 Conclusions

This study utilizes an advanced constitutive model to develop a 3D continuum FEM model. While the primary focus is on evaluating the constitutive models, the findings contribute to advancing numerical simulations for pile plunging, with further efforts made to consider large-deformation numerical solutions in the future. In addition, the parametric study for optimizing pile design in marl investigated the behavior of pile foundations in marl clay, focusing on the effects of critical state friction angle, pile side length, and embedment length on load-bearing performance. Key findings are listed below:

- The current FEM model generally captures the pile response in stiff marl; however, to fully simulate the entire process of pile plunging, large-deformation numerical solutions will need to be incorporated in future studies.
- The parametric study on the critical state friction angle (φ'_{cs}) showed that changes within the lower range (27° to 33°) had minimal impact on pile behavior. However, increasing φ'_{cs} to 35° and 37° significantly improved bearing capacity, indicating that even small increments at higher φ'_{cs} values can greatly enhance pile performance. This underscores the importance of precise soil characterization to optimize pile design in marl.
- The investigation into varying pile side lengths B (0.36 m, 0.46 m, 0.56 m) revealed that larger B significantly enhances load-bearing capacity, reduces displacement, and increases efficiency relative to size, providing greater overall load-bearing capacity.
- The study found that increasing embedment lengths (1.7 m, 3.4 m, 5.1 m) into marl enhances load-bearing capacity and reduces settlement. Although longer embedment generates more shaft resistance due to increased surface area, a smaller portion of the load is carried by shaft friction at greater depths, except at very low load levels.

References

Baus, R. L., and Ray, R. P. (1988). “Axial pile capacity study for piles in calcareous marl.” In Engineering for Calcareous Sediments Volume 1, CRC Press, 1st Ed., 7.

Bentley Systems, Inc. (2024). “PLAXIS 3D 2024.1 Material Models Manual 3D.” Bentley Systems.

Bentley Systems. (2023). “PLAXIS CONNECT Edition V21.00 User Defined Soil Models - OCClay: A Constitutive Model for Overconsolidated Clay based on the Hardening State Parameter.” Bentley Systems.

Brown, D., Dapp, S., Thompson, R., and Lazarte, C. (2007). “Geotechnical Engineering Circular No. 8 Design and Construction of Continuous Flight Auger (CFA) Piles.” Report FHWA-HIF-07-03, U.S. Department of Transportation, Washington, DC.

Camp, W. M., and Parmar, H. S. (1999). “Characterization of Pile Capacity with Time in the Cooper Marl: Study of Applicability of a Past Approach To Predict Long-Term Pile Capacity.” Transportation Research Record, 1663(1), 16-24.

Chen, Y., and Yang, Z. (2017). “A family of improved yield surfaces and their application in modeling of isotropically over-consolidated clays.” Computers and Geotechnics, 90, 133-143.

Davisson, M. T. (1972). “High capacity piles.” Proceedings of Soil Mechanics Lecture Series on Innovations in Foundation Construction, ASCE, Illinois Section, Chicago, 81-112.

Décourt, L. (1999). “Behaviour of foundations under working load conditions.” Proceedings of the 11th Pan-American Conference on Soil Mechanics and Geotechnical Engineering, Dolguassu, Brazil, 4, 453-488.

Fuller, F. M., and Hoy, H. E. (1970). “Pile load tests including quick load test method, conventional methods, and interpretations.” Research Record 333, Highway Research Board, Washington, DC, 74-86.

Gao, Z., Zhao, J., and Yin, Z. (2017). “A dilatancy relation for overconsolidated clay.” International Journal of Geomechanics, 17(5), 020.

Hueckel, T., Tatumluar, E., and Pellegrini, R. (1992). “A note on non-linear elasticity of isotropic overconsolidated clays.” International Journal for Numerical and Analytical Methods in Geomechanics, 16(6), 603-618.

Jocković, S., and Vukićević, M. (2017). “Bounding surface model for overconsolidated clays with new state parameter formulation of hardening rule.” Computers and Geotechnics, 83, 16-29.

Mayne, P.W., and Woeller, D.J. 2013. “Bored pile foundation response using seismic cone test data.” Proceedings of the 18th International Conference on Soil Mechanics and Geotechnical Engineering, Paris, Technical Committee 212 Deep Foundations.

Mita, K. A., Dasari, G. R., and Lo, K. W. (2004). “Performance of a three-dimensional Hvorslev-modified Cam-Clay model for overconsolidated clay.” International Journal of Geomechanics, 4(4), 296-309.

Murphy, G., Igoe, D., Doherty, P., and Gavin, K. (2018). "3D FEM approach for laterally loaded monopile design." Computers and Geotechnics, 100, 76-83.

Olgun, M., Yenginar, Y., and Hanati, A. (2017). “Interpreting load-settlement curves of pile foundations by graphical methods.”

Pender, M. (1978). “A model for the behaviour of overconsolidated soil.” Géotechnique, 28(1), 1-25.

Robertson, P. K. (2009). “Interpretation of cone penetration tests - A unified approach.” Can. Geotech. J., 46(11), 1337-1355.

Robertson, P. K., and Cabal, K. L. (2014). “Guide to Cone Penetration Testing for Geotechnical Engineering.” 6th Ed., Gregg Drilling & Testing, Inc.

U.S. Army Corps of Engineers. (1991). “Design of pile foundations.” Engineering Manual 1110-2-2906, Washington, DC 20314-1000.

Whittle, A. J. (1993). “Evaluation of a constitutive model for overconsolidated clays.” Géotechnique, 43(2), 289-313.

Yao, Y., Hou, W., and Zhou, A. (2008). “Constitutive model for overconsolidated clays.” Science in China Series E: Technological Sciences, 51(2), 179-191.

Yao, Y., Hou, W., and Zhou, A. (2009). “UH model: Three-dimensional unified hardening model for overconsolidated clays.” Géotechnique, 59(5), 451-469.

Chapter 4

4. Summary and Conclusions

4.1 Summary

This thesis comprehensively investigates the behavior of different piles in stiff marl under axial loads through field tests data and advanced numerical simulations. The key chapters are summarized as follows:

- Chapter 2 evaluates existing CPT-based methods and enhances them, analyzes pile load test data, and introduces numerical models using *t-z* and *Q-z* curves for predicting pile behavior and verifies these models with additional test piles.
- Chapter 3 details an 3D continuum FEM analysis using Plaxis 3D to capture strain-softening behavior, assess axial capacity, settlement behavior, and load transfer mechanisms. The chapter includes model calibration, validation, and a parametric study on marl's soil strength parameter and pile dimensions.

4.2 Conclusions

The following conclusions are drawn from this thesis:

Chapter 2:

- The original LCPC method exhibits significant errors when applied to marl due to its development for bored piles rather than driven piles, disregard for pore pressure on the CPT cone shoulder, use of vertical total stress instead of effective stress, and the imposition of unjustified upper limits on unit shaft resistance.

- The improved correlation coefficients for the LCPC method result in an error range of -13.7% to 7.2%, a significant improvement over the original coefficients, which underestimated pile resistance by up to 86.2%, leading to excessively conservative and costly designs.
- The improved correlation coefficients for the Eslami and Fellenius method result in errors ranging from -35.7% to -5.2%, providing a conservative estimate within an acceptable range. In contrast, the original coefficients led to overestimations of up to 52.1%.
- The calibrated *t-z* and *Q-z* curves developed in MATLAB generally yield accurate predictions of capacity, settlement, and load-transfer. Based on the verification results, using the shaft and toe resistance parameters correlated from both the LCPC and Eslami and Fellenius methods, the ultimate capacity shows an error of less than 10% compared to the pile load test results. Additionally, the load-transfer predictions match the pile load test results fairly well.

Chapter 3:

- The current FEM model generally captures the pile response in stiff marl; however, to fully simulate the entire process of pile plunging, large-deformation numerical solutions will need to be incorporated in future studies.
- The parametric study on the critical state friction angle (φ'_{cs}) showed that changes within the lower range (27° to 33°) had minimal impact on pile behavior. However, increasing φ'_{cs} to 35° and 37° significantly improved bearing capacity, indicating that even small increments at higher φ'_{cs} values can greatly enhance pile performance. This underscores the importance of precise soil characterization to optimize pile design in marl.

- The investigation into varying pile side lengths *B* (0.36 m, 0.46 m, 0.56 m) revealed that larger *B* significantly enhances load-bearing capacity, reduces displacement, and increases efficiency relative to size, providing greater overall load-bearing capacity.
- The study found that increasing embedment lengths (1.7 m, 3.4 m, 5.1 m) into marl enhances load-bearing capacity and reduces settlement. Although longer embedment generates more shaft resistance due to increased surface area, a smaller portion of the load is carried by shaft friction at greater depths, except at very low load levels.